arXiv:1010.3946v2 [hep-ph] 16 Feb 2011

Rescattering effects in $\eta \to 3\pi$ decays[*]

Sebastian P. Schneider, Bastian Kubis, Christoph Ditsche

Helmholtz-Institut für Strahlen- und Kernphysik (Theorie) and
Bethe Center for Theoretical Physics, Universität Bonn
Nußallee 14–16, D-53115 Bonn, Germany
E-mail: `schneider@hiskp.uni-bonn.de`, `kubis@hiskp.uni-bonn.de`,
    `ditsche@hiskp.uni-bonn.de`

ABSTRACT: The isospin-breaking decay $\eta \to 3\pi$ is an ideal tool to extract information on light quark mass ratios from experiment. For a precise determination, however, a detailed description of the Dalitz plot distribution is necessary. In that respect, in particular the slope parameter α of the neutral decay channel causes some concern, since the one-loop prediction from chiral perturbation theory misses the experimental value substantially. We use the modified non-relativistic effective field-theory, a dedicated framework to analyze final-state interactions beyond one loop including isospin-breaking corrections, to extract charged and neutral Dalitz plot parameters. Matching to chiral perturbation theory at next-to-leading order, we find $\alpha = -0.025 \pm 0.005$, in marginal agreement with experimental findings. We derive a relation between charged and neutral decay parameters that points towards a significant tension between the most recent KLOE measurements of these observables.

KEYWORDS: Chiral symmetries, Decays of other mesons, Meson–meson interactions.

Contents

1. Introduction

The decay $\eta \to 3\pi$ has been the center of attention in many theoretical and experimental works over the recent decades. The considerable interest is due to the fact that the decay can only occur via isospin-breaking operators and is therefore sensitive to the up- and down-quark mass difference. Indeed, the $\eta \to 3\pi$ transition amplitude is inversely proportional to the quark mass double ratio $\mathcal{Q}^2$,

$$\frac{1}{\mathcal{Q}^2} = \frac{m_d^2 - m_u^2}{m_s^2 - \hat{m}^2} \ , \qquad \hat{m} = \frac{1}{2}(m_u + m_d) \ , \tag{1.1}$$

and thus the decay provides an excellent testing ground for the breaking of chiral symmetry.

Despite valiant efforts it seemed difficult to bring theoretical description and experimental results in agreement. First attempts that relied on an electromagnetic transition [1,2] were unsuccessful in explaining the decay. SU(3) current algebra techniques in combination with the partially conserved axial-vector current hypothesis [3,4] were generalized to SU(3) chiral perturbation theory (ChPT) and initiated systematic improvements to the decay rate. While the one- and two-loop corrections to the decay were sizable [5,6], a consistent implementation of electromagnetic contributions only lead to small effects [7,8]. Despite these theoretical improvements the Dalitz plot expansion, especially of the neutral decay, remained an unsolved puzzle. The slope α vanishes at leading order, while at next-to-leading order ($\mathcal{O}(p^4)$, one loop) it disagrees in sign with experimental findings [9–17]. The same holds for the next-to-next-to-leading order ($\mathcal{O}(p^6)$, two loops) calculation [6]. The error on the final result is rather large, so that it allows for a negative slope parameter. However, this error is not based on the uncertainties due to the low-energy constants at $\mathcal{O}(p^6)$, which are estimated by resonance saturation, but results solely from the authors' fitting procedure.

It has been argued that $\pi\pi$ final-state interactions are the dominant force behind the sizable corrections [18,19], motivating several dispersive analyses [20–23] (see also Ref. [24]), which were able to give a more robust prediction of the slope parameter. Among the shortcomings of these dispersion relation techniques and the next-to-next-to-leading-order calculation is the treatment of higher-order isospin-breaking effects due to electromagnetism, as for example the mass difference between charged and neutral pions. It is not yet clear how to incorporate these effects.

An analysis of $\eta \to 3\pi$ in the framework of unitarized chiral perturbation theory has been conducted in Ref. [25], producing remarkable agreement with experiment. In particular, the experimental value of the slope parameter in the neutral decay channel can be accommodated. However, since this approach is based on an elaborate fitting procedure, wherein the U(3) expansion parameters are determined from several hadronic η and η' decay channels, among those $\eta \to 3\pi$, we do not consider this value for the slope parameter an unbiased *prediction*. Finally, a study of $\eta \to 3\pi$ in the framework of resummed ChPT is currently work in progress [26].

In this work we attempt to bridge the gap between the ChPT prediction and the dispersive analysis using the modified non-relativistic effective field theory framework (NREFT).

While this framework does not allow for a fundamental prediction of physical observables, it is ideally suited to study the dynamics of the final-state interactions. At two-loop accuracy and with the correct empirical $\pi\pi$ scattering parameters, we ought to have a reasonable approximation to the full dispersive resummation of rescattering effects at hand, so when matching to ChPT at $\mathcal{O}(p^4)$, we can hope to find a transparent interpretation of the dispersive results obtained in a similar fashion [20]. Additionally, the non-relativistic framework provides access to investigating the effects of isospin-breaking corrections.

This article is organized as follows. In Sect. 2 we begin with a short description of the Dalitz plot expansion and the conventions used throughout this work. An introduction to the non-relativistic framework, its power counting, the matching procedure, and numerical input is given in Sect. 3. Sections 4 and 5 comprise the analytic and numerical results in the isospin limit and with isospin breaking included. In Sect. 6 we study final-state interaction effects on an isospin relation between the charged and the neutral decay channel. In Sect. 7 finally, we briefly comment on the $\eta \to 3\pi$ partial widths and their ratio, before summarizing our findings in Sect. 8. Several of the more laborious formulae are relegated to the appendices.

2. Dalitz plot expansion of the decay amplitude

In the following we consider the charged and neutral decay modes

$$\eta(P_\eta) \to \pi^+(p_1)\pi^-(p_2)\pi^0(p_3) \ , \qquad s_1 + s_2 + s_3 = 3s_c = M_\eta^2 + 2M_\pi^2 + M_{\pi^0}^2 \ ,$$
$$Q_c = M_\eta - 2M_\pi - M_{\pi^0} \ ,$$
$$\eta(P_\eta) \to \pi^0(p_1)\pi^0(p_2)\pi^0(p_3) \ , \qquad s_1 + s_2 + s_3 = 3s_n = M_\eta^2 + 3M_{\pi^0}^2 \ ,$$
$$Q_n = M_\eta - 3M_{\pi^0} \ , \qquad (2.1)$$

where the kinematical variables are defined as $s_i = (P_\eta - p_i)^2$ with $p_i^2 = M_i^2$, $i = 1, 2, 3$, and $Q_{n/c}$ is the excess energy of the respective channel.[1] We will use the notation $M_\pi \doteq M_{\pi^\pm}$ throughout.

In experimental analyses of these decays, the squared absolute value of the amplitude is conventionally expanded as a polynomial around the center of the Dalitz plot in terms of symmetrized coordinates. For the charged decay channel one uses

$$x = \sqrt{3}\frac{E_2 - E_1}{Q_c} = \frac{s_1 - s_2}{\sqrt{3}R_c} \ , \qquad y = \frac{3E_3}{Q_c} - 1 = \frac{s_n - s_3}{R_c} + \delta \ , \qquad (2.2)$$

where $E_i = p_i^0 - M_i$ is the kinetic energy of i-th particle in the η rest frame, and we used the definitions

$$p_i^0 = \frac{M_\eta^2 + M_i^2 - s_i}{2M_\eta} \ , \qquad R_{c/n} = \frac{2}{3}M_\eta Q_{c/n} \ , \qquad \delta = \frac{Q_n}{Q_c} - 1 \ . \qquad (2.3)$$

---

[1]For convenience, we use a different notation from what is usually found in the literature. The transition can be made setting $s_1 = t$, $s_2 = u$, $s_3 = s$.

For the neutral channel one defines

$$z = \frac{2}{3}\sum_{i=1}^{3}\Big(\frac{3E_i}{Q_n} - 1\Big)^2 = \frac{2}{3}\sum_{i=1}^{3}\frac{(s_i - s_n)^2}{R_n^2} = x_n^2 + y_n^2 \ ,$$

$$x_n = \sqrt{z}\cos(\phi) \ , \quad y_n = \sqrt{z}\sin(\phi) \ , \tag{2.4}$$

where we have introduced polar coordinates in the center of the Dalitz plot. These definitions of x_n and y_n agree with x and y only for $M_\pi = M_{\pi^0}$. Experimental data is then fitted to the *Dalitz plot* distribution, which is of the form (assuming charge conjugation invariance)

$$|\mathcal{M}_c(x,y)|^2 = |\mathcal{N}_c|^2\big\{1 + ay + by^2 + dx^2 + fy^3 + gx^2y + \dots\big\} \ ,$$

$$|\mathcal{M}_n(z)|^2 = |\mathcal{N}_n|^2\big\{1 + 2\alpha z + 2\beta z^{3/2}\sin(3\phi) + 2\gamma z^2 + \dots\big\} \ , \tag{2.5}$$

where a, b, d, f, g and α, β, γ are the Dalitz plot parameters and $\mathcal{N}_c$, $\mathcal{N}_n$ are the normalizations of the charged and the neutral decay, respectively. We note that of the higher-order parameters beyond quadratic order in x and y, only f has been measured so far (by the KLOE collaboration [27]). However, with the advent of very high statistics measurements for $\eta \to 3\pi^0$ e.g. at MAMI [28], a determination of β and γ might not be beyond the realm of possibility.

We wish to comment on the validity of the polynomial expansion Eq. (2.5) in particular for the neutral decay channel. The boundary of the Dalitz plot for $\eta \to 3\pi^0$ is shown in Fig. 1. The dotted lines denote the three symmetry axes, the dotted circle depicts the beginning of the rapid decrease of pure phase space for radii $\sqrt{z} > \sqrt{0.756}$. It is important to note that the cusps due to $\pi^+\pi^- \to \pi^0\pi^0$ final state rescattering occur at $s_i = 4M_\pi^2$ and not at a single z value; the smallest and the largest values of z crossing the cusp lines ($z = 0.598$ and $z = 0.882$, respectively) are indicated at the corresponding arrows. Therefore the polynomial representation for the neutral Dalitz plot distribution (2.5) is only valid for $z < 0.598$, i.e. inside the dashed circle.

Figure 1: Boundary of the $\eta \to 3\pi^0$ Dalitz plot. Dotted: symmetry axes and biggest enclosed circle. Dashed: cusps at $s_i = 4M_\pi^2$ and corresponding circle. Arrows: indicating specific z values (see text for details).

Table 1 summarizes the latest experimental determinations and theoretical predictions for α. In the following we propose an explanation for the disagreement between the ChPT result and experimental data. Our findings substantiate the dispersive result [20], and
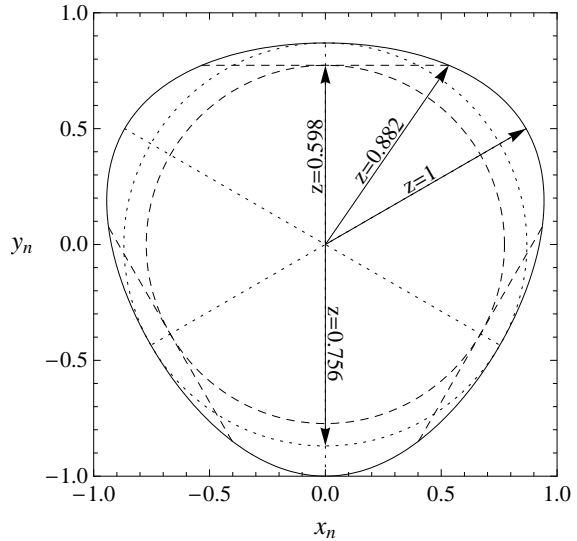
we are confident that it leads to a better understanding of the nature of the final-state interactions.

It is worthwhile at this point to quote the ChPT decay amplitudes at leading order p^2 and up to next-to-leading order in the isospin-breaking parameters $m_d - m_u$ and e^2. For the charged and neutral decay, respectively, they read [8] (we use the Condon–Shortley phase convention throughout)

$$\mathcal{M}_c^{\text{LO}}(s_1, s_2, s_3) = \frac{B_0(m_d - m_u)}{3\sqrt{3}F_\pi^2}\left\{1 + \frac{3(s_3 - s_n)}{M_\eta^2 - M_{\pi^0}^2}\right\} ,$$
$$\mathcal{M}_n^{\text{LO}}(s_1, s_2, s_3) = -\frac{B_0(m_d - m_u)}{\sqrt{3}F_\pi^2} , \tag{2.6}$$

where $F_\pi = 92.2$ MeV is the pion decay constant, and B_0 is linked to the quark condensate in the (SU(3)) chiral limit in the standard manner. Equation (2.6) shows the isospin-violating nature of the decay, as both leading-order amplitudes are explicitly of order $m_d - m_u$. At that order in isospin breaking, the $\eta \to 3\pi$ amplitudes fulfill the well-known $\Delta I = 1$ relation

$$\mathcal{M}_n(s_1, s_2, s_3) = -\mathcal{M}_c(s_1, s_2, s_3) - \mathcal{M}_c(s_2, s_3, s_1) - \mathcal{M}_c(s_3, s_1, s_2) , \tag{2.7}$$

which can be easily checked in Eq. (2.6). This relation even holds in general at leading order in the isospin-breaking parameters, i.e. also for terms of $\mathcal{O}(e^2)$ [7], and is only violated at $\mathcal{O}((m_d - m_u)e^2)$ [8]. In the following, we will often adopt a loose way of talking and speak about the *isospin limit* for the charged and neutral $\eta \to 3\pi$ amplitudes; this only refers to the approximation in which the relation Eq. (2.7) holds, in particular $M_{\pi^0} = M_\pi$, and *not* to the limit $m_u = m_d$, where the decay $\eta \to 3\pi$ is (almost) forbidden.

Note furthermore that all contributions involving $\Delta_\pi = M_\pi^2 - M_{\pi^0}^2 = \mathcal{O}(e^2)$ in the charged decay amplitude have been absorbed by writing Eq. (2.6) in terms of s_n. This motivates an expansion of the decay amplitudes of *both* channels around the point $s_3 = s_n$, $s_1 = s_2$: we anticipate that, defined this way, higher-order isospin-breaking corrections to the $\Delta I = 1$ rule for the normalization of the amplitude are going to be of chiral order p^4, without contributions from the tree-level amplitudes Eq. (2.6), and therefore small. This "center" of the Dalitz plot then corresponds to $s_1 = s_2 = s_3 = s_n$ and $x_n = y_n = z = 0$ in the neutral channel, but to $s_1 = s_2 = s_n + \Delta_\pi$, $s_3 = s_n$ or $x = 0$ and $y = \delta \neq 0$ in the charged case. The charged and neutral decay amplitudes then take the form

$$\mathcal{M}_c(s_1, s_2, s_3) = \tilde{\mathcal{N}}_c\Big\{1 + \tilde{a}(s_3 - s_n) + \tilde{b}(s_3 - s_n)^2 + \tilde{d}(s_1 - s_2)^2 + \tilde{f}(s_3 - s_n)^3$$
$$+ \tilde{g}(s_1 - s_2)^2(s_3 - s_n) + \dots\Big\}$$
$$= \mathcal{N}_c\Big\{1 + \bar{a}y + \bar{b}y^2 + \bar{d}x^2 + \bar{f}y^3 + \bar{g}x^2y + \dots + \mathcal{O}\big((R_n - R_c)^2\big)\Big\} ,$$
$$\mathcal{M}_n(s_1, s_2, s_3) = \mathcal{N}_n\Big\{1 + \tilde{\alpha}\big[(s_1 - s_n)^2 + (s_2 - s_n)^2 + (s_3 - s_n)^2\big]$$
$$+ \tilde{\beta}\big[(s_1 - s_n)^3 + (s_2 - s_n)^3 + (s_3 - s_n)^3\big]$$
$$+ \tilde{\gamma}\big[(s_1 - s_n)^4 + (s_2 - s_n)^4 + (s_3 - s_n)^4\big] + \dots\Big\}$$

Theory	α
ChPT $\mathcal{O}(p^4)$ [5]	$+0.013$
ChPT $\mathcal{O}(p^6)$ [6]	$+0.013 \pm 0.032$
Dispersive [20]	$-0.007 \ldots -0.014$
Experiment	α
Crystal Ball@BNL [9]	-0.031 ± 0.004
Crystal Barrel@LEAR [10]	-0.052 ± 0.020
GAMS-2000 [11]	-0.022 ± 0.023
KLOE [12]	$-0.0301 \pm 0.0035^{+0.0022}_{-0.0035}$
MAMI-B [13]	$-0.032 \pm 0.002 \pm 0.002$
MAMI-C [14]	-0.032 ± 0.003
SND [15]	$-0.010 \pm 0.021 \pm 0.010$
WASA@CELSIUS [16]	$-0.026 \pm 0.010 \pm 0.010$
WASA@COSY [17]	$-0.027 \pm 0.008 \pm 0.005$

Table 1: Theoretical predictions and experimental findings on the slope parameter α.

$$= \mathcal{N}_n \Big\{ 1 + \bar{\alpha} z + \bar{\beta} z^{3/2} \sin(3\phi) + \bar{\gamma} z^2 + \ldots \Big\} . \tag{2.8}$$

The relations between the expansion parameters up to first order in isospin breaking are found to be

$$\mathcal{N}_c = \bar{\mathcal{N}}_c \times \tilde{\mathcal{N}}_c , \qquad \bar{\mathcal{N}}_c = 1 + \tilde{a}(R_n - R_c) ,$$

$$\bar{a} = -R_c \frac{\tilde{a} + 2(R_n - R_c)\tilde{b}}{\bar{\mathcal{N}}_c} , \quad \bar{b} = R_c^2 \frac{\tilde{b} + 3(R_n - R_c)\tilde{f}}{\bar{\mathcal{N}}_c} , \quad \bar{d} = 3R_c^2 \frac{\tilde{d} + \tilde{g}(R_n - R_c)}{\bar{\mathcal{N}}_c} ,$$

$$\bar{f} = -\frac{R_c^3 \tilde{f}}{\bar{\mathcal{N}}_c} , \quad \bar{g} = -\frac{3R_c^3 \tilde{g}}{\bar{\mathcal{N}}_c} , \quad \bar{\alpha} = \frac{3}{2} R_n^2 \tilde{\alpha} , \quad \bar{\beta} = \frac{3}{4} R_n^3 \tilde{\beta} , \quad \bar{\gamma} = \frac{9}{8} R_n^4 \tilde{\gamma} . \tag{2.9}$$

The expansion in powers of $R_n - R_c \simeq 3.35 \times 10^{-3}$ GeV^2 hinges on the fact that we have considered isospin breaking corrections in the definition of y (in the isospin limit, $R_n = R_c$, we reproduce the results derived in Ref. [6]). The relations to the Dalitz plot parameters of the squared value of the respective amplitudes Eq. (2.5) are then easily shown to be

$$a = 2\,\mathrm{Re}(\bar{a}) , \qquad b = |\bar{a}|^2 + 2\,\mathrm{Re}(\bar{b}) , \qquad d = 2\,\mathrm{Re}(\bar{d}) , \qquad f = 2\,\mathrm{Re}(\bar{a}\bar{b}^* + \bar{f}) ,$$

$$g = 2\,\mathrm{Re}(\bar{a}\bar{d}^* + \bar{g}) , \qquad \alpha = \mathrm{Re}(\bar{\alpha}) , \qquad \beta = \mathrm{Re}(\bar{\beta}) , \qquad \gamma = \mathrm{Re}(\bar{\gamma}) . \tag{2.10}$$

The $\Delta I = 1$ rule Eq. (2.7) gives rise to relations between Dalitz plot parameters and normalizations of the neutral and the charged decay amplitude, namely

$$\mathcal{N}_n = -3\tilde{\mathcal{N}}_c , \qquad \tilde{\alpha} = \frac{1}{3}(\tilde{b} + 3\tilde{d}) . \tag{2.11}$$

3. The modified non-relativistic effective field theory framework

In this work we will use the modified non-relativistic effective field theory (NREFT) framework to analyze the final-state interactions in $\eta \to 3\pi$. This framework provides a useful tool to investigate low-energy scattering and decay processes: it has found applications in detailed studies of cusp effects in $K \to 3\pi$ [29–31] and $\eta \to 3\pi$ [32] as well as $\eta' \to \eta\pi\pi$ [33] decays, and has recently been extended to describe near-threshold pion photo- and electroproduction on the nucleon [34, 35] (for an overview on cusp effects in meson decays, see Ref. [36]).

An analysis of $\eta \to 3\pi$ within the non-relativistic framework is useful for the following reasons. While the non-relativistic amplitude is perturbative, just as the chiral amplitude, it allows for a more accurate implementation of $\pi\pi$ interactions due to the inclusion of phenomenological threshold parameters as determined from Roy equations. Non-perturbative treatments, as for example dispersive analyses, are expected to yield yet more precise results. Compared to such numerically very involved studies, however, the NREFT calculation leads to a very transparent analytic representation. Moreover, it allows for the direct implementation of isospin breaking in particular in all kinematic effects, which is much more involved in ChPT and unexplored in dispersive analyses.

In that context it is useful to narrow down the precise definition of the term "non-relativistic" as it is used in our work. Our representation of the decay amplitude is only non-relativistic in the sense that inelastic thresholds outside the physical region are subsumed into point-like effective coupling constants. Inside the physical region, however, we arrive at a fully covariant expression with the correct non-analytic low-energy behavior. The number of low-energy Dalitz plot couplings to be included in the Lagrangian at tree-level is modeled after the traditional (experimental) Dalitz plot expansion, which seems to yield a rather good description of the experimental data in the center of the Dalitz plot. We note again, see Sect. 2, that the *full* Dalitz plot is not accurately described by a polynomial expansion, since such a representation neglects non-analytic effects, such as cusps at the opening of the charged pion threshold (see also Refs. [8, 30, 32]).

In fact, the non-relativistic approach to $\eta \to 3\pi$ is not new. In Ref. [32] the authors performed a fit to experimental data in an attempt to investigate the cusp effect in $\eta \to 3\pi^0$ generated at the opening of the charged pion threshold. The scope of our work is entirely different. We focus specifically on an analysis of the Dalitz plot parameters based on numerical input parameters derived from ChPT. For that endeavor the amplitudes are calculated to yet-higher accuracy in order to ensure the incorporation of the most prominent effects generated by the final-state interactions. In the following section we give a brief introduction to the modified non-relativistic framework.

3.1 Power counting (1): basics and tree amplitudes

A Lagrangian treatment of $\eta \to 3\pi$ in the non-relativistic framework is provided in Ref. [30] and will not be repeated here. Instead, we will briefly comment on the power counting and outline the basic features of the amplitudes of $\eta \to 3\pi$ and the $\pi\pi$ final-state interactions.

A consistent power counting scheme for the modified non-relativistic effective field theory is constructed by introducing the formal non-relativistic parameter ϵ and count

- pion 3-momenta (in the η rest frame) as $\mathcal{O}(\epsilon)$,

- kinetic energies $T_i = p_i^0 - M_i$ as $\mathcal{O}(\epsilon^2)$,

- masses of the particles involved as $\mathcal{O}(1)$, but $\Delta_\pi = M_\pi^2 - M_{\pi^0}^2$ as $\mathcal{O}(\epsilon^2)$,

- and the excess energy $Q_{n/c} = \sum_i T_i$ as $\mathcal{O}(\epsilon^2)$.

Loop corrections in the perturbative series involve $\pi\pi$ rescattering at not-too-high energies, which can be related to the effective range expansion of the $\pi\pi$ amplitude. Since these effective range parameters are phenomenologically small, we use them as an additional power counting parameter, referred to generically as $a_{\pi\pi}$. We thus have a correlated expansion in $a_{\pi\pi}$ and ϵ and can uniquely assign powers to our loop expansion (for a more detailed introduction to the modified non-relativistic effective field theory we refer to Refs. [29–31]).

Following the previous counting scheme a Lagrangian framework can be constructed. From that the $\eta \to 3\pi$ amplitude at tree level can be derived as

$$\mathcal{M}_n^{\text{tree}}(s_1, s_2, s_3) = K_0 + K_1 \Big[(p_1^0 - M_{\pi^0})^2 + (p_2^0 - M_{\pi^0})^2 + (p_3^0 - M_{\pi^0})^2 \Big] + \mathcal{O}(\epsilon^6) \ ,$$

$$\mathcal{M}_c^{\text{tree}}(s_1, s_2, s_3) = L_0 + L_1(p_3^0 - M_{\pi^0}) + L_2(p_3^0 - M_{\pi^0})^2 + L_3(p_1^0 - p_2^0)^2 + \mathcal{O}(\epsilon^6) \ , \quad (3.1)$$

where the low-energy couplings K_i, L_i are of $\mathcal{O}(1)$ and are related to the traditional Dalitz plot, see Sect. 3.3. The isospin relation Eq. (2.7) translates into

$$K_0 = -(3L_0 + L_1 Q_n - L_3 Q_n^2) \ , \qquad K_1 = -(L_2 + 3L_3) \ . \quad (3.2)$$

The number of constants included here corresponds to expanding the Dalitz plot up to quadratic order; we briefly comment on the possible inclusion of cubic terms at tree level in Sect. 4.2. We remark that the number of four independent tree-level couplings (in the isospin limit) chosen here equals the number of subtraction constants in several of the dispersive analyses [21, 22] (compare Ref. [23], though). Analogously, the $\pi\pi$ scattering amplitude can be determined. We consider the following final-state processes (i) ($\pi^a \pi^b \to \pi^c \pi^d$): (00) (00; 00), ($x$) (+−; 00), (+0) (+0; +0), and (+−) (+−; +−). Up to $\mathcal{O}(a_{\pi\pi}^2 \epsilon^2)$ the threshold expansion of the amplitudes in the respective channels are given as

$$\text{Re}\, T_{NR}^{00} = 2C_{00} + 2D_{00}(s - s_{00}^{\text{thr}}) + 2F_{00}(s - s_{00}^{\text{thr}})^2 + 4C_x^2 J_{+-}(s) + \dots \ ,$$

$$\text{Re}\, T_{NR}^{x} = 2C_x + 2D_x(s - s_x^{\text{thr}}) + 2F_x(s - s_x^{\text{thr}})^2 + \dots \ ,$$

$$\text{Re}\, T_{NR}^{+0} = 2C_{+0} + 2D_{+0}(s - s_{+0}^{\text{thr}}) + 2F_{+0}(s - s_{+0}^{\text{thr}})^2 - E_{+0}(t - u) + \dots \ ,$$

$$\text{Re}\, T_{NR}^{+-} = 2C_{+-} + 2D_{+-}(s - s_{+-}^{\text{thr}}) + 2F_{+-}(s - s_{+-}^{\text{thr}})^2 - E_{+-}(t - u) + \dots \ , \quad (3.3)$$

where s_i^{thr} denotes the threshold of the pertinent channel, $s_{00}^{\text{thr}} = 4M_{\pi^0}^2$, $s_x^{\text{thr}} = 4M_\pi^2$, $s_{+0}^{\text{thr}} = (M_{\pi^0} + M_\pi)^2$, $s_{+-}^{\text{thr}} = 4M_\pi^2$. The one-loop function of the non-relativistic theory,

$$J_{+-}(s) = \frac{i}{16\pi} \sqrt{1 - \frac{4M_\pi^2}{s}} \ , \quad (3.4)$$

is responsible for a cusp structure in the (00)-channel (see Refs. [29, 37] for further details). The low-energy couplings are matched to the effective range expansion in the following section.

3.2 Matching (1): $\pi\pi$ scattering

We want to make more sense of the low-energy couplings introduced in the previous section. To determine the matching relations for the low-energy constants of $\pi\pi$ scattering, we resort to the effective range expansion of the $\pi\pi$ scattering amplitude, which is conventionally decomposed into partial waves according to

$$T_I(s,t) = 32\pi \sum_l (2l+1) t_l^I(s) P_l(z) , \tag{3.5}$$

where $t_l^I(s)$ is the partial wave amplitude of angular momentum l and isospin I, $P_l(z)$ are the Legendre polynomials, and $z = \cos\theta$ is the cosine of the scattering angle in the center-of-mass system. Close to threshold the partial wave amplitude can be expanded in terms of the center-of-mass momentum $q^2 \doteq q^2(s) = (s - 4M_\pi^2)/4$, leading to

$$\mathrm{Re}\, t_l^I(s) = q^{2l}\{a_l^I + b_l^I q^2 + c_l^I q^4 + \mathcal{O}(q^6)\} , \tag{3.6}$$

where a_l^I is the scattering length, b_l^I is the effective range, and c_l^I is the (leading) shape parameter. In the following we use the simplified notation a_I, b_I, c_I, as only S- and P-waves will be considered. In the language of NREFT power counting the previous equation is an expansion in orders of ϵ, since $q^2 \propto \epsilon^2$. The effective range expansion is thus naturally related to the non-relativistic $\pi\pi$ scattering amplitude in Eq. (3.3), and we can read off the matching relations for the low-energy couplings, shown here for simplicity in the isospin limit:

$$
\begin{aligned}
C_{00} &= \frac{16\pi}{3}(a_0 + 2a_2) , & D_{00} &= \frac{4\pi}{3}(b_0 + 2b_2) , & F_{00} &= \frac{\pi}{3}(c_0 + 2c_2) , & & \tag{3.7}\\
C_x &= \frac{16\pi}{3}(-a_0 + a_2) , & D_x &= \frac{4\pi}{3}(-b_0 + b_2) , & F_x &= \frac{\pi}{3}(-c_0 + c_2) , & & \\
C_{+0} &= 8\pi a_2 , & D_{+0} &= 2\pi b_2 , & F_{+0} &= \frac{\pi}{2}c_2 , & E_{+0} &= 12\pi a_1 , \\
C_{+-} &= \frac{8\pi}{3}(2a_0 + a_2) , & D_{+-} &= \frac{2\pi}{3}(2b_0 + b_2) , & F_{+-} &= \frac{\pi}{6}(2c_0 + c_2) , & E_{+-} &= 12\pi a_1 .
\end{aligned}
$$

Isospin-breaking corrections to these matching relations are discussed in Appendix A.1. Note that Eq. (3.7) is only valid up to $\mathcal{O}(a_{\pi\pi}^2)$, i.e. $\pi\pi$ scattering to one loop, or $\eta \to 3\pi$ to two loops. At higher loop orders, the low-energy couplings D_i and F_i are renormalized, which we will briefly discuss in the context of higher-loop resummation at the end of Sect. 4.1.

We will use two sets of phenomenological values for the $\pi\pi$ effective range parameters, the combined Roy equation plus ChPT analysis of Refs. [38, 39] (henceforth denoted by ACGL) and a combination of forward dispersion relations and Roy equations [40] (KPY). The central or "best" values for S- and P-wave scattering lengths and effective ranges as obtained in those two analyses are quoted in Table 2. The determination of the shape

parameters is a little more delicate. We use the respective parameterizations of the phase shifts given in Refs. [38, 40] and calculate the scattering amplitude according to

$$\mathrm{Re}\, t_0^I(q^2) = \left(1 + \frac{M_\pi^2}{q^2}\right)^{1/2} \frac{\tan \delta_I}{1 + \tan^2 \delta_I} \ , \qquad I = 0,\, 2 \ . \tag{3.8}$$

Since the shape parameters are numerically very small in comparison to effective ranges and scattering lengths, they are rather sensitive to the method by which they are determined.

For example, one receives rather different results when extracting the shape parameter from a strict threshold expansion of the amplitude, or from a fit over a certain low-energy range, minimizing the χ^2-function

$$\chi^2(c_I) = \left(\mathrm{Re}\, t_0^I(q^2) - a_I - b_I q^2 - c_I q^4\right)^2 \ , \tag{3.9}$$

in a range from the threshold $4M_\pi^2$ up to the expansion point s_n. Furthermore, the inclusion of an additional term $d_I q^6$ causes significant deviations in the $I = 0$ channel, since this term and the leading shape parameter are of comparable size. We decide to use the central values obtained from the minimization of Eq. (3.9) as the most reasonable approximation to the true partial wave. The numerical results for $c_{0,2}$ thus obtained are also given in Table 2. In the following,

	ACGL	KPY
a_0	0.220	0.223
a_2	-0.0444	-0.0444
$b_0 \times M_\pi^2$	0.276	0.290
$b_2 \times M_\pi^2$	-0.0803	-0.081
$c_0 \times 10^2 M_\pi^4$	-0.19	0.04
$c_2 \times 10^2 M_\pi^4$	1.33	0.68
$a_1 \times 10 M_\pi^2$	0.379	0.381
$b_1 \times 10^2 M_\pi^4$	0.567	0.512

Table 2: Input values for the scattering lengths a_I, effective ranges b_I, and shape parameters c_I as determined from the two parameterizations ACGL [38, 39] and KPY [40] (see text for discussion).

we use the variation between the central values of the two parameterizations [38, 40] as a means to estimate the uncertainty due to $\pi\pi$ rescattering.

3.3 Matching (2): $\eta \to 3\pi$

We compare Eqs. (2.8) and (3.1) to derive the matching relation between the low-energy couplings of the $\eta \to 3\pi$ tree amplitude and the traditional Dalitz plot parameterization, namely

$$
\begin{aligned}
K_0 &= \tilde{\mathcal{N}}_n^{\mathrm{tree}} \left(1 - 3\tilde{\alpha}^{\mathrm{tree}} R_n^2\right) \ , & K_1 &= 4\tilde{\mathcal{N}}_n^{\mathrm{tree}} M_\eta^2 \tilde{\alpha}^{\mathrm{tree}}, \\
L_0 &= \tilde{\mathcal{N}}_c^{\mathrm{tree}} (1 + \tilde{a}^{\mathrm{tree}} R_n + \tilde{b}^{\mathrm{tree}} R_n^2) \ , & L_1 &= -2\tilde{\mathcal{N}}_c^{\mathrm{tree}} M_\eta (\tilde{a}^{\mathrm{tree}} + 2\tilde{b}^{\mathrm{tree}} R_n) \ , \\
L_2 &= 4\tilde{\mathcal{N}}_c^{\mathrm{tree}} M_\eta^2 \tilde{b}^{\mathrm{tree}} \ , & L_3 &= 4\tilde{\mathcal{N}}_c^{\mathrm{tree}} M_\eta^2 \tilde{d}^{\mathrm{tree}} \ ,
\end{aligned}
\tag{3.10}
$$

where the superscript "tree" denotes tree-level input parameters. Note that Eq. (3.10) fulfills the isospin relation Eq. (3.2) as long as Eq. (2.11) is satisfied. To extract the Dalitz plot parameters in the non-relativistic framework, we have to fix the numerical input for the tree-level low-energy couplings for the $\eta \to 3\pi$ amplitude. We determine the low-energy couplings of the Dalitz plot in Eq. (3.10) by matching the non-relativistic framework to the one-loop ChPT amplitude [5] at the center of the Dalitz plot. Following Ref. [8], we evaluate the chiral $\eta \to 3\pi$ amplitude using *neutral* masses everywhere.

We remark that the upcoming [22] (and previous [21]) dispersive analyses use the Adler zero of the $\eta \to \pi^+\pi^-\pi^0$ amplitude as the matching point, compare Eq. (2.6). It is protected by SU(2) symmetry and therefore not prone to large strange-quark-mass corrections. The chiral series is thus expected to converge rather quickly, which makes the Adler zero a natural choice. The fact that it lies outside the physical region at roughly $s_A \approx \frac{4}{3}M_\pi^2$, however, renders matching the non-relativistic framework to the chiral amplitude at this point ill-fated: the expansion in terms of ϵ does not necessarily converge there, and we therefore have to resort to matching inside the Dalitz plot.

For the matching procedure we tune the rescattering parameters in the non-relativistic amplitude in such a way as to mimic the chiral amplitude. In essence this means that the scattering lengths and effective ranges are fixed at their current algebra values (this corresponds to the insertion of $\mathcal{O}(p^2)$ vertices in the chiral expansion). Explicitly, we have

$$a_0^{\mathrm{CA}} = \frac{7M_\pi^2}{32\pi F_\pi^2} \ , \qquad a_2^{\mathrm{CA}} = -\frac{M_\pi^2}{16\pi F_\pi^2} \ , \qquad a_1^{\mathrm{CA}} = \frac{1}{24\pi F_\pi^2} \ ,$$
$$b_0^{\mathrm{CA}} = \frac{1}{4\pi F_\pi^2} \ , \qquad b_2^{\mathrm{CA}} = -\frac{1}{8\pi F_\pi^2} \ . \tag{3.11}$$

We proceed analogously with the $\eta \to 3\pi$ couplings that enter the non-relativistic amplitude at one-loop level and derive from Eq. (2.6)

$$\tilde{\mathcal{N}}_c^{\mathrm{LO}} = -\frac{(M_\eta^2 - M_\pi^2)(M_\pi^2 + 3M_\eta^2)}{16\mathcal{Q}^2\sqrt{3}F_\pi^2 M_\pi^2} \ , \qquad \tilde{a}^{\mathrm{LO}} = \frac{3}{M_\eta^2 - M_\pi^2} \ . \tag{3.12}$$

For our numerical analysis we will use the value for $\mathcal{Q}$ dictated by Dashen's theorem, $\mathcal{Q}_D = 24.2$. Note that the specific choice does not hold any ramifications for our main statements, since it merely enters in the normalization, which drops out in the Dalitz plot parameters.

The above matching procedure is consistent as it ensures that the imaginary parts are exclusively generated by $\pi\pi$ final-state interactions. Residual effects from the chiral pion loops are purely real and absorbed in the low-energy couplings. We use matching to $\mathcal{O}(p^4)$ and not to $\mathcal{O}(p^6)$ for practical reasons: the above matching procedure is simpler and our results can be used to compare with and interpret the dispersive analyses directly. A high-precision determination of the Dalitz plot parameters would likely require matching to $\mathcal{O}(p^6)$, but for that purpose the low-energy constants showing up at $\mathcal{O}(p^6)$ may not be known with sufficient accuracy. Numerically we obtain from matching to the ChPT amplitude at $\mathcal{O}(p^4)$ (using the chiral SU(3) low-energy constant[2] $L_3^{\mathrm{r}} = -3.5 \times 10^{-3}$ [41])

$$\tilde{\mathcal{N}}_c^{\mathrm{tree}} = -0.158 \ , \qquad\qquad \tilde{a}^{\mathrm{tree}} = 13.428 \ \mathrm{GeV}^{-2} \ ,$$
$$\tilde{b}^{\mathrm{tree}} = -7.291 \ \mathrm{GeV}^{-4} \ , \qquad\qquad \tilde{d}^{\mathrm{tree}} = 5.189 \ \mathrm{GeV}^{-4} \ . \tag{3.13}$$

The particle masses used throughout this work are given by the current particle data group values [42], i.e. $M_\pi = 139.57$ MeV, $M_{\pi^0} = 134.98$ MeV, and $M_\eta = 547.86$ MeV.

---

[2]The effects of varying L_3^{r} within its error were checked to be tiny compared to other uncertainties. We therefore only use the central value.

3.4 Power counting (2): loops and $\eta \to 3\pi$

The power counting scheme discussed in Sect. 3.1 gives rise to a natural decomposition of the NREFT amplitude. This can be seen as follows. The modified non-relativistic propagator counts as $\mathcal{O}(\epsilon^{-2})$ (see e.g. Ref. [29]), the loop integration measure (with one energy and three momentum integration variables) as ϵ^5, therefore any loop integral with two-body rescattering contributes at $\mathcal{O}(\epsilon)$. Moreover, such a loop always involves a $\pi\pi$ rescattering vertex and is thus of $\mathcal{O}(a_{\pi\pi})$. The decomposition of the full $\eta \to 3\pi$ amplitude according to its loop-structure,

$$\mathcal{M}_{n/c}(s_1, s_2, s_3) = \mathcal{M}_{n/c}^{\text{tree}}(s_1, s_2, s_3) + \mathcal{M}_{n/c}^{\text{1-loop}}(s_1, s_2, s_3) + \mathcal{M}_{n/c}^{\text{2-loop}}(s_1, s_2, s_3) + \dots \ , \quad (3.14)$$

is thus an expansion in powers of $a_{\pi\pi}\epsilon$. There is an interesting simplification of Eq. (3.14) close to the center of the Dalitz plot ($s_1 \approx s_2$, $s_3 \approx s_n$) above all two-pion thresholds. The contribution of the one-loop function is purely imaginary as can be seen from Eq. (3.4). At the same time the two-loop bubble diagram, which is the product of two one-loop functions, is purely real and it can be shown that the imaginary part of the non-trivial two-loop function does not contribute at this order (see for example Refs. [29, 30]). Symbolically we can write both amplitudes in terms of the power counting parameter $a_{\pi\pi}$,

$$\mathcal{M} = \mathcal{M}_{\text{tree}} + i\mathcal{M}_{\text{1-loop}}a_{\pi\pi} + \mathcal{M}_{\text{2-loop}}a_{\pi\pi}^2 + \mathcal{O}(ia_{\pi\pi}^3\epsilon^3, ia_{\pi\pi}^2\epsilon^4) \ , \quad (3.15)$$

where the $\mathcal{O}(ia_{\pi\pi}^2\epsilon^4)$ term stems from the three-particle cut at two-loop order, which is numerically small as discussed in Appendix C and therefore neglected. By taking the absolute value squared we obtain

$$|\mathcal{M}|^2 = \mathcal{M}_{\text{tree}}^2 + (\mathcal{M}_{\text{1-loop}}^2 + \mathcal{M}_{\text{tree}} \times \mathcal{M}_{\text{2-loop}})a_{\pi\pi}^2 + \mathcal{O}(a_{\pi\pi}^4\epsilon^4, a_{\pi\pi}^3\epsilon^5) \ . \quad (3.16)$$

We therefore expect one- and two-loop effects to be of the same size at the center of the Dalitz plot, as only the two-loop contributions can interfere with the dominant tree terms there, and thus to impact the Dalitz plot parameters about equally.

The heightened importance of rescattering effects in Dalitz plot parameters is further substantiated by another observation. Consider the generic one-loop function of $\pi\pi$ rescattering in the non-relativistic theory expanded about the center of the Dalitz plot ($s = s_n$, we neglect isospin-breaking effects in the following discussion, so that $M_{\pi^0} = M_\pi$):

$$J(s) = \frac{i\sqrt{1 - \frac{4M_\pi^2}{s_n}}}{16\pi}\left(1 + \frac{6M_\pi^2}{s_n}\frac{s - s_n}{M_\eta^2 - 9M_\pi^2} - \frac{18M_\pi^2(s_n - 3M_\pi^2)}{s_n^2}\left(\frac{s - s_n}{M_\eta^2 - 9M_\pi^2}\right)^2 + \dots\right)$$

$$= \mathcal{O}(\epsilon) \ , \quad (3.17)$$

since $s - s_n = \mathcal{O}(\epsilon^2)$ and $M_\eta - 3M_\pi = \mathcal{O}(\epsilon^2)$. The same holds true for the two-loop functions. This implies that contributions to higher-order Dalitz plot parameters from the loop functions are enhanced non-analytically in $M_\eta - 3M_\pi$. We conclude from Eq. (3.16)

$$\mathcal{M}_{\text{1-loop}}^2 + \mathcal{M}_{\text{tree}} \times \mathcal{M}_{\text{2-loop}} = \mathcal{O}(\epsilon^2) \ , \quad (3.18)$$
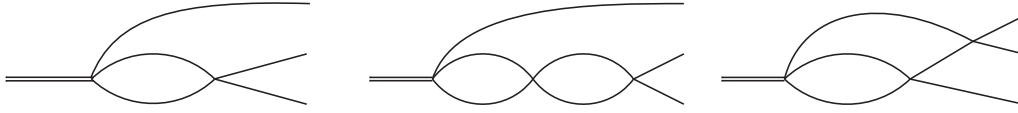
Figure 2: The Feynman graph topologies at one and two loops contributing to the decay $\eta \to 3\pi$ in NREFT. The double line denotes the η particle, the single lines stand for pions (of arbitrary charges).

which has substantial consequences for the slope parameter α of the neutral decay channel. We can parameterize the slope parameter according to

$$\alpha = \alpha_0 + \alpha_2 a_{\pi\pi}^2 + \mathcal{O}(a_{\pi\pi}^4) \ . \tag{3.19}$$

From relations Eq. (3.10) we find $\tilde{\alpha}^{\text{tree}} = \mathcal{O}(1)$ and consequently the slope parameter at tree-level is of order $\alpha_0 \propto Q_n^2 \tilde{\alpha}^{\text{tree}} = \mathcal{O}(\epsilon^4)$, whereas rescattering effects enter the slope parameter at $\mathcal{O}(a_{\pi\pi}^2 \epsilon^2)$. This obviously implies that rescattering effects become increasingly more important for higher-order Dalitz plot parameters. On the other hand, they are far less significant (as we will confirm numerically below) for the normalization of the amplitude, for which we expect higher-order quark-mass renormalization effects to be more important.

The full NREFT representation beyond tree level with isospin breaking included is given in Appendix B. It comprises the loop graph topologies displayed in Fig. 2, and is fully consistent in terms of non-relativistic power counting up-to-and-including $\mathcal{O}(a_{\pi\pi}^2 \epsilon^4)$, i.e. the vertices of the two-loop graphs are included at $\mathcal{O}(\epsilon^2)$. Phenomenologically, one finds that the expansions of the $\eta \to 3\pi$ and $\pi\pi \to \pi\pi$ polynomials in powers of ϵ^2 only converge well starting from next-to-next-to-leading order, i.e. the $\mathcal{O}(\epsilon^2)$ terms (the linear slope in $\eta \to \pi^+\pi^-\pi^0$ and the $\pi\pi$ effective ranges) are not really suppressed compared to the leading (constant) terms. This observation is readily understood resorting to chiral perturbation theory: due to the Goldstone nature of the pions, the constant terms are chirally suppressed by powers of M_π^2 and the leading $\mathcal{O}(p^2)$ amplitudes are linear in energy s. In other words, the $\mathcal{O}(\epsilon^2)$ contributions are "suppressed" versus the constant ones by factors of s/M_π^2, and only starting from $\mathcal{O}(\epsilon^4)$, the relative suppression is s/Λ_χ^2 with $\Lambda_\chi \approx 1$ GeV. The chiral two-loop or $\mathcal{O}(p^6)$ calculation [6] contains all the leading $\mathcal{O}(p^2)$ vertices and therefore the linear $\eta \to 3\pi$ slope as well as effective ranges for the $\pi\pi$ interaction (although not quite the phenomenologically accurate ones). In order to guarantee that our NREFT representation of the decay amplitude is at least as accurate as the chiral two-loop one, we include all combinations of linear energy dependences in the three vertices of the two-loop diagrams. Thus, our amplitude also contains terms that are of $\mathcal{O}(a_{\pi\pi}^2 \epsilon^6)$ and $\mathcal{O}(a_{\pi\pi}^2 \epsilon^8)$, and due to the enhancement discussed above, the numerically most important ones appearing at those orders. The representation of the "double bubbles" (see also Fig. 2) is even strictly complete up to $\mathcal{O}(a_{\pi\pi}^2 \epsilon^6)$, as P-wave contributions only start at $\mathcal{O}(a_{\pi\pi}^2 \epsilon^8)$. Furthermore, we have added shape parameter terms in the "double bubbles" and in the outer vertex of the irreducible two-loop graph, where the addition of these terms is trivial.

4. The isospin limit

We first give an analytic and numerical treatment of the amplitude in the isospin limit, which we *define* as $M_{\pi^0} = M_\pi$ and using Eq. (3.2). This already includes the gross features of our total analysis. However, in the isospin limit, we can give relatively simple closed analytic expressions for all parts of the amplitudes up to two loops.

4.1 Structure of the amplitude

The non-relativistic decay amplitude (for the charged channel) can be split into parts consisting of tree and final-state contributions

$$\mathcal{M}_c(s_1, s_2, s_3) = \mathcal{M}_c^{\text{tree}}(s_1, s_2, s_3) + \mathcal{M}_c^{\text{fsi}}(s_1, s_2, s_3) , \tag{4.1}$$

where the tree amplitude is given by

$$\mathcal{M}_c^{\text{tree}}(s_1, s_2, s_3) = \tilde{\mathcal{N}}_c^{\text{tree}}\left\{1 + \tilde{a}^{\text{tree}}(s_3 - s_n) + \tilde{b}^{\text{tree}}(s_3 - s_n)^2 + \tilde{d}^{\text{tree}}(s_1 - s_2)^2\right\} , \tag{4.2}$$

and the rescattering contributions of the amplitude can be decomposed up to $\mathcal{O}(p^8)$ according to the isospin structure of the final-state pions [21, 43, 44],

$$\mathcal{M}_c^{\text{fsi}}(s_1, s_2, s_3) = \mathcal{M}_0(s_3) + (s_3 - s_1)\mathcal{M}_1(s_2) + (s_3 - s_2)\mathcal{M}_1(s_1)$$
$$+ \mathcal{M}_2(s_1) + \mathcal{M}_2(s_2) - \frac{2}{3}\mathcal{M}_2(s_3) , \tag{4.3}$$

where the index $I = 0, 1, 2$ of the function $M_I(s_i)$ denotes the total isospin of the respective kinematic channel. At $\mathcal{O}(a_{\pi\pi}^2 \epsilon^4)$ (for details see Sect. 3.4) the isospin amplitudes are given as

$$\mathcal{M}_0(s) = \frac{5}{3}\left\{\ell_0(s)J(s)\left(1 + 16\pi a_0(s)J(s)\right)\right.$$
$$+ \frac{32\pi}{3}\left[\left(\ell_0'(s)a_0(\tilde{s}) + 2\ell_2'(s)a_2(\tilde{s})\right)F^{(0)}(s) + \left(\frac{2L_1}{M_\eta}\left(\frac{2}{5}a_0(\tilde{s}) - a_2(\tilde{s})\right) - \ell_0'(s)b_0\right.\right.$$
$$\left.\left.\left. - 2\ell_2'(s)b_2\right)\frac{M_\eta \mathbf{Q}^2}{2Q^0}F^{(1)}(s) - 2L_1\left(\frac{2}{5}b_0 - b_2\right)\frac{M_\eta \mathbf{Q}^4}{4Q^{0^2}}F^{(2)}(s)\right]\right\}16\pi a_0(s) ,$$

$$\mathcal{M}_1(s) = \left\{-\frac{q^2\ell_1(s)}{M_\eta}J(s) + \frac{80\pi s}{M_\eta Q^0}\left[\left(\ell_0'(s)a_0(\tilde{s}) - \ell_2'(s)a_2(\tilde{s})\right)\left(F^{(0)}(s) - 2F^{(1)}(s)\right)\right.\right.$$
$$+ \left(\frac{L_1}{M_\eta}\left(\frac{4}{5}a_0(\tilde{s}) + a_2(\tilde{s})\right) - \ell_0'(s)b_0 + \ell_2'(s)b_2\right)\frac{M_\eta \mathbf{Q}^2}{2Q^0}\left(F^{(1)}(s) - 2F^{(2)}(s)\right)$$
$$\left.\left. - L_1\left(\frac{4}{5}b_0 + b_2\right)\frac{M_\eta \mathbf{Q}^4}{4Q^{0^2}}\left(F^{(2)}(s) - 2F^{(3)}(s)\right)\right]\right\}4\pi a_1(s) ,$$

$$\mathcal{M}_2(s) = \left\{\ell_2(s)J(s)\left(1 + 16\pi a_2(s)J(s)\right)\right.$$
$$+ \frac{16\pi}{3}\left[\left(5\ell_0'(s)a_0(\tilde{s}) + \ell_2'(s)a_2(\tilde{s})\right)F^{(0)}(s) + \left(\frac{4L_1}{M_\eta}\left(a_0(\tilde{s}) - \frac{a_2(\tilde{s})}{4}\right) - 5\ell_0'(s)b_0\right.\right.$$
$$\left.\left.\left. - \ell_2'(s)b_2\right)\frac{M_\eta \mathbf{Q}^2}{2Q^0}F^{(1)}(s) - 4L_1\left(b_0 - \frac{b_2}{4}\right)\frac{M_\eta \mathbf{Q}^4}{4Q^{0^2}}F^{(2)}(s)\right]\right\}16\pi a_2(s) , \tag{4.4}$$

where the various polynomials are given by

$$\ell_0(s) = \frac{3}{5}\ell(s) + \frac{2}{5}\ell_2(s) , \quad \ell(s) = L_0 + L_1\left(p^0 - M_\pi\right) + L_2\left(p^0 - M_\pi\right)^2 + L_3\frac{4\mathbf{Q}^2}{3s}\,q^2 ,$$

$$\ell_2(s) = L_0 + L_1\left(\frac{Q^0}{2} - M_\pi\right) + L_2\left[\left(\frac{Q^0}{2} - M_\pi\right)^2 + \frac{\mathbf{Q}^2}{3s}q^2\right] + L_3\left[\left(\frac{Q^0}{2} - p^0\right)^2 + \frac{\mathbf{Q}^2}{3s}q^2\right] ,$$

$$\ell_1(s) = L_1 + 2L_2\left(\frac{Q^0}{2} - M_\pi\right) + 2L_3\left(p^0 - \frac{Q^0}{2}\right) , \quad \ell'_0(s) = \frac{3}{5}\ell'(s) + \frac{2}{5}\ell'_2(s) ,$$

$$\ell'(s) = L_0 + L_1\left(\frac{s}{2Q^0} - M_\pi\right) , \quad \ell'_2(s) = L_0 + L_1\left(\frac{M_\eta}{2} - M_\pi - \frac{s}{4Q^0}\right) ,$$

$$a_I(s) = a_I + b_I q^2 + c_I q^4 , \tag{4.5}$$

and we use the kinematic variables

$$p^0 = \frac{M_\eta^2 + M_\pi^2 - s}{2M_\eta} , \quad Q^0 = \frac{M_\eta^2 - M_\pi^2 + s}{2M_\eta} , \quad \mathbf{Q}^2 = \frac{\lambda(M_\eta^2, M_\pi^2, s)}{4M_\eta^2} ,$$

$$\tilde{s} = 2M_\pi^2 - s + \frac{M_\eta}{Q^0}\left(s + 2\mathbf{Q}^2\right) , \tag{4.6}$$

with the Källén function $\lambda(x, y, z) = x^2 + y^2 + z^2 - 2(xy + yz + zx)$. Note that the shape parameter terms $\propto c_I$ are to be omitted in $a_I(\tilde{s})$; we also neglect them in the $I = 1$ partial wave. We use the shorthand expressions $J(s) \doteq J_{+-}(s)$ and $F^{(n)}(s) \doteq F_+^{(n)}(M_\pi, M_\pi, M_\pi, M_\pi, s)$ (in the isospin limit), where for the exact form of the two-loop functions we refer to Appendix B. We can now write the Dalitz plot parameters in terms of the isospin amplitudes, namely for the charged channel

$$\mathcal{N}_c = \tilde{\mathcal{N}}_c^{\text{tree}} + \mathcal{M}_0(s_n) + \frac{4}{3}\mathcal{M}_2(s_n) ,$$

$$\bar{a} = -\frac{R_c}{\mathcal{N}_c}\left(\tilde{\mathcal{N}}_c^{\text{tree}}\tilde{a}^{\text{tree}} + \mathcal{M}_0^{(1)}(s_n) + 3\mathcal{M}_1(s_n) - \frac{5}{3}\mathcal{M}_2^{(1)}(s_n)\right) ,$$

$$\bar{b} = \frac{R_c^2}{\mathcal{N}_c}\left(\tilde{\mathcal{N}}_c^{\text{tree}}\tilde{b}^{\text{tree}} + \frac{1}{2}\mathcal{M}_0^{(2)}(s_n) - \frac{3}{2}\mathcal{M}_1^{(1)}(s_n) - \frac{1}{12}\mathcal{M}_2^{(2)}(s_n)\right) ,$$

$$\bar{d} = \frac{3R_c^2}{\mathcal{N}_c}\left(\tilde{\mathcal{N}}_c^{\text{tree}}\tilde{d}^{\text{tree}} + \frac{1}{2}\mathcal{M}_1^{(1)}(s_n) + \frac{1}{4}\mathcal{M}_2^{(2)}(s_n)\right) ,$$

$$\bar{f} = -\frac{R_c^3}{\mathcal{N}_c}\left(\frac{1}{6}\mathcal{M}_0^{(3)}(s_n) + \frac{3}{8}\mathcal{M}_1^{(2)}(s_n) - \frac{11}{72}\mathcal{M}_2^{(3)}(s_n)\right) ,$$

$$\bar{g} = -\frac{3R_c^3}{8\mathcal{N}_c}\left(\mathcal{M}_1^{(2)}(s_n) - \mathcal{M}_2^{(3)}(s_n)\right) , \tag{4.7}$$

and for the neutral channel

$$\bar{\alpha} = \frac{R_n^2}{4\mathcal{N}_c}\left(2\tilde{\mathcal{N}}_c^{\text{tree}}\left(\tilde{b}^{\text{tree}} + 3\tilde{d}^{\text{tree}}\right) + \mathcal{M}_0^{(2)}(s_n) + \frac{4}{3}\mathcal{M}_2^{(2)}(s_n)\right) ,$$

$$\bar{\beta} = \frac{R_n^3}{24\mathcal{N}_c}\left(\mathcal{M}_0^{(3)}(s_n) + \frac{4}{3}\mathcal{M}_2^{(3)}(s_n)\right) ,$$

$$\bar{\gamma} = \frac{R_n^4}{64\mathcal{N}_c}\left(\mathcal{M}_0^{(4)}(s_n) + \frac{4}{3}\mathcal{M}_2^{(4)}(s_n)\right) , \tag{4.8}$$
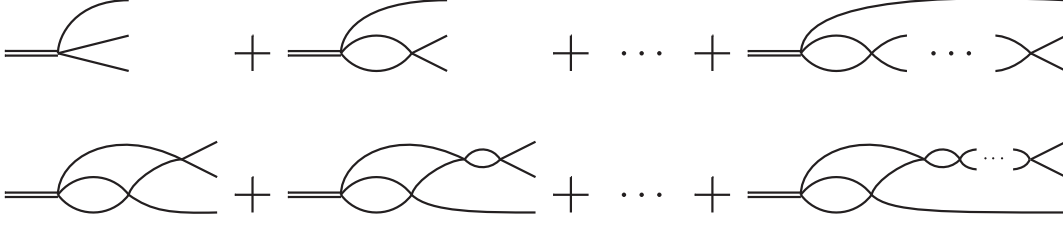
Figure 3: Diagrammatic expression of the resummed amplitudes. Above: the bubble chain. Below: resummed external vertex of the non-trivial two-loop graph. The line style is as in Fig. 2.

where $\mathcal{M}_I^{(n)}(s_n)$ denotes the n-th derivative of the function $\mathcal{M}_I(s)$, evaluated at the center of the Dalitz plot. Note that $\bar{d}$ and $\bar{g}$ do not receive contributions from the isospin $I = 0$ amplitude.

Despite working in the limit of evaluating all amplitudes for the *charged* pion mass, we employ the physical values for R_c and R_n in Eqs. (4.7), (4.8). These prefactors stem from the conversion of $\tilde{a}$, $\tilde{\alpha}$ etc. into $\bar{a}$, $\bar{\alpha}$ etc., see Eq. (2.9), and are just due to a normalization choice in the definition of the Dalitz plot variables x and y; we therefore decide to present our results including this "trivial" isospin-breaking effect already at this stage. Note that due to $(M_\eta - 3M_{\pi^0})/(M_\eta - 3M_\pi) \approx 1.11$ and $(M_\eta - 2M_\pi - M_{\pi^0})/(M_\eta - 3M_\pi) \approx 1.04$, the effects of using these normalization factors in the isospin limit are large, most so for the neutral channel, where α for instance is affected by a shift of 22%.

In our numerical analysis we will observe that among the two-loop contributions those of the non-trivial two-loop graphs, see Fig. 2 (right), are in general strongly suppressed. This can be traced back to the isospin properties of these pieces: for those Dalitz plot parameters to which the $I = 0$ partial wave can contribute, it usually dominates. For those graphs that only describe rescattering in one channel and can be written as simple products of one-loop functions, see Fig. 2 (middle), the $I = 0$ isospin amplitude receives contributions proportional to second powers of a_0, b_0, etc., whereas the "inner" vertex in the non-trivial two-loop contributions has parts of $I = 0$ and $I = 2$ (P-waves vanish due to symmetry reasons in the isospin limit) that tend to partially cancel each other. In an attempt to estimate (partial) higher-order corrections, we therefore expect to find a good approximation to the full result by iterating the bubble diagrams and the exterior two-particle rescattering of the non-trivial two-loop function as depicted diagrammatically in Fig. 3. In the aforementioned representation the unitarized amplitudes are easily determined to be

$$\mathcal{M}_0^{\mathrm{u}}(s) = \frac{\mathcal{M}_0(s) - \frac{5}{3}\ell_0(s)\big(16\pi a_0(s)J(s)\big)^2}{1 - 16\pi a_0(s)J(s)} \ ,$$

$$\mathcal{M}_1^{\mathrm{u}}(s) = \frac{\mathcal{M}_1(s)}{1 - 16\pi a_1(s)q^2 J(s)} \ ,$$

$$\mathcal{M}_2^{\mathrm{u}}(s) = \frac{\mathcal{M}_2(s) - \ell_2(s)\big(16\pi a_2(s)J(s)\big)^2}{1 - 16\pi a_2(s)J(s)} \ . \tag{4.9}$$

The inclusion of iterated diagrams requires modified matching relations for the effective

range parameters. This becomes obvious when considering the expansion of the iterated bubble sum of $\pi\pi$ scattering of isospin $I = 0, 2$ at the $\pi\pi$ threshold:

$$\mathrm{Re}\left[\frac{a_I(s)}{1 - 16\pi a_I(s)J(s)}\right] = a_I + \left(b_I - \frac{a_I^3}{M_\pi^2}\right)q^2 + \left(c_I + \frac{a_I^3 + a_I^5 - 3a_I^2 b_I M_\pi^2}{M_\pi^4}\right)q^4 + \mathcal{O}(q^6) \ . \tag{4.10}$$

One immediately sees that the effective range picks up a contribution from two-loop diagrams, the shape parameter from two- and four-loop diagrams. To account for this shift, the above expression has to be compared with the effective range expansion of the $\pi\pi$ amplitude (for $l = 0$),

$$\mathrm{Re}\, t_0^I(q^2) = a_I + b_I q^2 + c_I q^4 + \mathcal{O}(q^6) \ , \qquad I = 0, 2 \ , \tag{4.11}$$

from which one reads off the following renormalization prescriptions:

$$a_I^{\mathrm{ren}} = a_I \ , \qquad b_I^{\mathrm{ren}} = b_I + \frac{a_I^3}{M_\pi^2} \ , \qquad c_I^{\mathrm{ren}} = c_I - \frac{a_I^3 - 2a_I^5 - 3a_I^2 b_I M_\pi^2}{M_\pi^4} \ . \tag{4.12}$$

The a_I^{ren}, b_I^{ren}, c_I^{ren} are now to be inserted into the matching relations for the coupling constants C_i, D_i, F_i. The renormalization prescriptions have pretty remarkable effects in the isospin $I = 0$ channel, where the shape parameter is shifted from $-0.002 M_\pi^{-4}$ to $+0.030 M_\pi^{-4}$ (for the ACGL parameter set). We note that the P-wave effective range b_1 does not pick up an additional contribution due to the $q^2(s)$ prefactor. Corrections in the P-wave channel start at $\mathcal{O}(\epsilon^8)$, that is the higher-order shape parameter d_1.

4.2 Numerical results

We begin our numerical analysis of the various $\eta \to 3\pi$ Dalitz plot parameters by investigating how the tree-level values are modified at one- and two-loop order, and finally beyond two loops (via the estimate through the unitarized amplitudes in Eq. (4.9)). This part of the analysis is based solely on the ACGL parameters for the $\pi\pi$ final-state interaction; the qualitative conclusions are identical for the KPY parameterization. We keep the $\eta \to 3\pi$ tree level parameters fixed as obtained by matching to ChPT at $\mathcal{O}(p^4)$ throughout, see Sect. 3.3. Our results are summarized in Table 3. In particular, we observe the following:

1. Individual loop corrections to the Dalitz plot parameters are sizeable; their relative importance grows with increasing order (in ϵ) of the parameters concerned, as suggested a priori by power-counting arguments (see Sect. 3.4).

2. One- and two-loop contributions are in general of the same size, as indeed expected, with a tendency to cancel to varying extent due to contributions of opposite sign. This again substantiates the power-counting arguments of the NREFT framework, which is particularly interesting in the case of α: while at one loop we see a sizeable positive shift added to the already positive tree-level result, the two-loop correction overwhelms both, leading to a negative total. We therefore find the correct sign for α, as opposed to the ChPT result. At two loops our result is in fairly good agreement with the dispersive one from Ref. [20].

	charged channel					
	$\|\mathcal{N}_c\|^2$	a	b	d	f	g
tree	0.0310	−1.306	0.393	0.071	0.022	−0.046
one-loop	0.0338	−1.450	0.580	0.085	−0.026	−0.078
two-loop*	0.0289	−1.288	0.334	0.093	0.078	−0.076
full two-loop	0.0287	−1.290	0.379	0.056	0.071	−0.045
unitarized	0.0284	−1.268	0.342	0.053	0.101	−0.042

	neutral channel		
	$\|\mathcal{N}_n\|^2$	α	β	γ
tree	0.279	0.0107	0	0.0001
one-loop	0.304	0.0227	0.0005	0.0000
two-loop*	0.260	−0.0209	−0.0027	0.0007
full two-loop	0.258	−0.0192	−0.0036	0.0009
unitarized	0.255	−0.0249	−0.0043	0.0013

Table 3: Results for the charged and neutral Dalitz plot parameters in the isospin limit. We show tree, one-loop, two-loop neglecting the irreducible two-loop graphs (marked "two-loop*"), and full two-loop results calculated as described in the text, plus the result employing the unitarized amplitudes according to Eq. (4.9).

3. There are large contributions from derivative couplings at two-loop order. This is seen when considering the amplitude expanded only up to $\mathcal{O}(a_{\pi\pi}\epsilon^5, a_{\pi\pi}^2\epsilon^2)$ (cf. Ref. [30]), at which order only constant vertices are implemented at two loops. In this approximation, we find numerically e.g. $\alpha = +0.033$. Once the effective range corrections in the $I = 0$ two-loop bubble are added, α receives a shift to -0.017. This observation explains why the authors of Ref. [32] obtain a positive sign for α when matching to ChPT at tree-level: no derivative couplings at two-loop level are included in that work. With respect to this omission, matching to ChPT at tree-level plays a minor role in the deviation from our result.

4. By comparing the two-loop contributions with and without the parts due to the irreducible two-loop graphs, see Fig. 2 (right), we see that at least in those parameters that receive contributions from the $I = 0$ amplitude the irreducible two-loop graphs only give a very small contribution. As detailed before, this can be traced back to the isospin structure of the different amplitudes. Specifically α is a case in point: the simple "bubble sum" type two-loop graphs shift it by about -0.044, while the irreducible graphs only add $+0.002$.

5. Our estimate of higher-order effects via simple two-channel unitarization shows that

	ACGL 2-loop	ACGL unit.	KPY 2-loop	KPY unit.	average
$\lvert\mathcal{N}_c\rvert^2$	0.0287	0.0284	0.0285	0.0282	0.0284 ± 0.0002
a	-1.290	-1.268	-1.291	-1.267	-1.279 ± 0.012
b	0.379	0.342	0.382	0.340	0.361 ± 0.021
d	0.056	0.053	0.052	0.050	0.053 ± 0.003
f	0.071	0.101	0.073	0.107	0.089 ± 0.018
g	-0.045	-0.042	-0.043	-0.041	-0.043 ± 0.002
α	-0.0192	-0.0249	-0.0227	-0.0291	-0.0242 ± 0.0049
β	-0.0036	-0.0043	-0.0043	-0.0051	-0.0043 ± 0.0007
γ	0.0009	0.0013	0.0013	0.0017	0.0013 ± 0.0004

Table 4: Results for charged and neutral Dalitz plot parameters in the isospin limit with different input on $\pi\pi$ scattering parameters from Refs. [38] and [40]; see Sect. 3.2. Shown are the results both for two loops and for the unitarized amplitudes. $\lvert\mathcal{N}_n\rvert^2 = 9\lvert\mathcal{N}_c\rvert^2$ is not shown separately.

those are significantly smaller than the (individual) one- and two-loop effects, although not negligible throughout. Due to the smallness of the irreducible two-loop graphs, we expect to catch the major part of the higher-order corrections in this way.

In order to study the dependence of our results on the precise input for $\pi\pi$ scattering, we next compare the values obtained for the various charged and neutral Dalitz plot parameters, at two loops and unitarized, for the ACGL and the KPY parameter sets in Table 4. In most cases, the variation with different $\pi\pi$ input is a bit smaller than the difference due to the higher-order estimates, although not by much. As our final result in the last column of Table 4, we determine central values and (symmetric) errors in such a way as to cover all four values for each parameter.

Our finding for the $\eta \to 3\pi^0$ slope parameter, $\alpha = -0.024 \pm 0.005$, is considerably closer to the current experimental average $\alpha = -0.0317 \pm 0.0016$ [42] than previous theoretical approaches. Note again that the theoretical prediction for α is lowered (in absolute value) by about 22% if the charged pion mass is used in the definition of z. We predict the (yet unmeasured) higher-order Dalitz plot parameters β and γ in the neutral channel to be different from zero, but very small. In particular, neglecting a term $\propto \gamma z^2$ in an experimental extraction of α based on the radial distribution $d\Gamma/dz$ alone (in which a term $\propto \beta$ cancels for $z < 0.756$, compare Fig. 1) should affect α by less than the value of γ, hence still below the current uncertainty, although not by much given the precision of the most recent experimental determinations.

As we will see below, there are sizeable isospin-breaking shifts in the charged Dalitz plot parameters. We therefore defer a detailed comparison to experimental values to Sect. 5. We only wish to make a remark on the cubic parameters f and g here. Apart from the fact that a large contribution to these is given by $2\mathrm{Re}(\bar{a}\bar{b}^*)$ and $2\mathrm{Re}(\bar{a}\bar{d}^*)$, respectively, the remainders (or $\bar{f}$, $\bar{g}$) are given entirely in terms of loop contributions. If we, in addition,

allow for cubic tree level terms $\bar{f}^{\text{tree}}$ and $\bar{g}^{\text{tree}}$ and match the latter to ChPT at $\mathcal{O}(p^4)$, the total results receive shifts of -0.002 and -0.011 hence very and relatively small effects, respectively. Although chiral $\mathcal{O}(p^6)$ corrections might modify these numbers significantly, we still regard them as indications that the dominance of loop contributions (as suggested by ϵ power counting) holds here.

4.3 Comparison to α in ChPT at two loops

While dispersive analyses find values for α similar to ours [20], a serious puzzle is the question why the calculation of this quantity in ChPT to two loops [6] does not arrive at least at a negative value for α "naturally", i.e. as the central value (disregarding the large error bar due to the estimated fit uncertainty). After all, in addition to potentially significant chiral SU(3) renormalization effects of what would be subsumed in the tree-level couplings of the NREFT representation, ChPT at $\mathcal{O}(p^6)$ also includes all the pion two-loop graphs shown to be important here.

It turns out that this failure of the chiral two-loop calculation can partly be understood within our framework, investigating rescattering effects only, but of course neglecting the $\mathcal{O}(p^6)$ modified tree-level couplings. In order to mimic the chiral expansion, we note that in an $\mathcal{O}(p^6)$ calculation, the $\pi\pi$ vertices inside two-loop graphs are only included to their current-algebra (or $\mathcal{O}(p^2)$) accuracy, see Eq. (3.11), while inside the one-loop diagrams, $\pi\pi$ rescattering is taken care of up to $\mathcal{O}(p^4)$. By inserting the respective values for the $\pi\pi$ threshold parameters in our amplitude, we find

$$\alpha_{\text{ChPT}} = -0.0011 \ , \tag{4.13}$$

hence a value close to zero. We attribute the remaining difference to the central result for α in Ref. [6] to different tree-level couplings as determined in that paper. As we found that precisely the two-loop effects turn α negative, dominated by the $I = 0$ amplitude, we conclude that a large part of the discrepancy between ChPT at $\mathcal{O}(p^6)$ and our result (or the one from dispersion relations) is due to the significantly weaker $\pi\pi$ rescattering (compare e.g. $a_0^{\text{CA}} \approx 0.16$ vs. $a_0 = 0.220$ from Ref. [38], which enters the two-loop effects squared). The precise choice of the set of rescattering parameters therefore has a large effect on the result for α (and, slightly less dramatically so, on other Dalitz plot parameters). The inclusion of improved values for the effective ranges and shape parameters produces a large shift of the chiral result towards the experimental value.

In a very condensed manner, we can therefore point to one specific diagram, Fig. 2 (middle), which accounts for roughly half of the discrepancy between the central value of the chiral prediction at $\mathcal{O}(p^6)$ and the experimental value for α. More specifically, the discrepancy is caused by contributions of the diagrammatic topology of this kind. Since (at least) next-to-leading order contributions to the $\pi\pi$ vertices are required, one needs to include these diagrams up to $\mathcal{O}(p^8)$ and higher in strict chiral power counting. To substantiate this claim and ensure that it is not an artifact of the non-relativistic framework, we replace the non-relativistic two-point function $J(s)$, Eq. (3.4), by its relativistic counterpart $\bar{J}_{\pi\pi}(s)$, which differs from the former by its real part (given explicitly in Eq. (A.11)).

Doing so requires a different matching procedure to account for the (otherwise absent) mass renormalization effects on the various coupling constants thus induced; we will not spell out this exercise in detail. The main conclusion however is fully consistent with our findings above: the "double bubble" graphs alone shift α by -0.042 (to be compared with -0.044, see Table 3); calculating them with current algebra values for the $\pi\pi$ threshold parameters reduces this effect by nearly a factor of two, which corresponds to the discrepancy between Eq. (4.13) and the value obtained in NREFT.

One might argue that a parameter as subtle as α could also be subject to other very sizeable $\mathcal{O}(p^6)$ corrections; in particular, contributions from chiral low-energy constants appear for the first time at that order. For a superficial impression of these effects, we investigate precisely the $\mathcal{O}(p^6)$ polynomial in the amplitude calculated in Ref. [6]. One easily finds the following combination of low-energy constants contributing to α:

$$\alpha_{\text{LEC}}^{(6)} = \frac{12R_n^2}{F_\pi^4}\big(C_5^r + C_8^r + 3C_9^r + C_{10}^r - 2C_{12}^r + 2C_{22}^r + 3C_{24}^r + C_{25}^r\big) \ . \tag{4.14}$$

The couplings C_i^r are estimated in Ref. [6] using resonance saturation. Vector contributions cancel in Eq. (4.14), as they must, with no P-waves appearing in the neutral decay channel. Using the scalar resonance estimates given in Ref. [6], we arrive at the very simple and compact expression

$$\alpha_{\text{LEC}}^{(6)} = \frac{12R_n^2 c_d c_m}{F_\pi^2 M_S^4} \approx 0.005 \ , \tag{4.15}$$

where $c_m = 0.042$ GeV, $c_d = 0.032$ GeV, and $M_S = 0.98$ GeV. There are serious doubts about the reliability of the resonance saturation hypothesis in the scalar sector [45]; indeed on might argue that the masses of even heavier scalar states ought to be used in Eq. (4.15), further suppressing their contribution to α. We nevertheless confirm that contributions from the ChPT low-energy polynomial at $\mathcal{O}(p^6)$ are rather small; in particular they have a positive sign, so they cannot serve as an alternative explanation to arrive at a negative α. We also emphasize that the above is only a very rough estimate of the expected size of the effects and does not by any means replace a consistent matching procedure.

5. Isospin breaking in $\eta \to 3\pi$

In this section we discuss higher-order isospin-breaking contributions to the decay $\eta \to 3\pi$. We concentrate on the following four contributions:

1. Isospin breaking in $\eta \to \pi^+\pi^-\pi^0$ due to $Q_n \neq Q_c$. There are significant corrections to the charged Dalitz plot parameters due to the terms $\propto (R_n - R_c)$ in Eq. (2.9), which stem from the subtleties in the definition of the center of the Dalitz plot discussed in Sect. 2.

2. Other isospin corrections due to the difference between the charged and the neutral pion mass. These in particular concern the incorporation of the correct thresholds inside the loop contributions, which is necessary for a description of the boundary

regions of the Dalitz plot, among them the cusp effect in $\eta \to 3\pi^0$. The representation of the amplitude in the non-relativistic framework allows us to work in the particle (and not in the isospin) basis, and thus we can incorporate mass effects in a straightforward fashion.

3. Isospin-breaking corrections to the $\pi\pi$ rescattering parameters. We use the phenomenological values for the scattering lengths and effective ranges, which have been determined in the isospin limit [38, 40], and calculate corrections to each channel from the one-loop SU(2) $\pi\pi$-scattering amplitudes with electromagnetic corrections included.

4. Next-to-leading-order isospin-breaking effects in the $\eta \to 3\pi$ tree level couplings, calculated in one-loop ChPT, which modify Eqs. (2.11).

The representation of the NREFT amplitude to two loops with fully general masses and coupling constants, allowing for all of these isospin-breaking effects, is given in Appendix B.1. Furthermore Appendix B.2 shows the generalization of the unitarization prescription given in Eq. (4.9) for the case of isospin violation. In our numerical evaluation we will add these contributions cumulatively to the results of Sect. 4.

In this context we should comment on radiative (real- and virtual-photon) corrections to these decays. In order to be able to sensibly discuss a Dalitz plot expansion of the squared amplitudes in question, we assume that the universal radiative corrections (Gamow–Sommerfeld factor, bremsstrahlung contributions etc.), as discussed in the framework of NREFT in Ref. [31], have already been subtracted from the experimental data when determining Dalitz plot parameters. In order to extract the corrections of point 4 above from the calculation in Ref. [8], these subtracted contributions have to be matched correctly, as detailed in Appendix A.2. The non-universal or "internal" radiative corrections that play an important role in the analysis of the cusp effect in $K \to 3\pi$ [31, 46] do not have a similarly enhanced effect in the center of the Dalitz plot. From the point of view of chiral power counting of isospin-breaking corrections, these constitute higher-order effects than those considered consistently in Ref. [8] (as they only appear at two loops); furthermore, in $\eta \to \pi^+\pi^-\pi^0$, even diagrams beyond those calculated in Ref. [31] would have to be included. We have checked, though, that the effect of photon exchange inside the charged-pion loops on the $\eta \to 3\pi^0$ Dalitz plot expansion is small, even on the scale of the other small isospin-breaking effects discussed below.

The by far largest isospin-breaking effects on the Dalitz plot parameters, beyond the use of the correct overall normalization factors of Q_n and Q_c in the definitions of the kinematic variables that was already incorporated in the previous sections, are the kinematic effects due to the fact that for the decay $\eta \to \pi^+\pi^-\pi^0$ the position defined by $x = y = 0$ does not coincide with $s_1 = s_2 = s_3$ when $M_\pi \neq M_{\pi^0}$. Using the correct prescriptions given in Eq. (2.9), we find the results listed in the left column of Table 5. The corrections are very sizeable: our analysis shows that a is reduced (in magnitude) by 5%, b by even 14%. These kinematic effects constitute the bulk of the isospin breaking corrections to the charged parameters.

	$Q_c \neq Q_n$	masses	$\pi\pi$	$\eta \to 3\pi^0$
$|\mathcal{N}_c|^2$	0.0310 ± 0.0003	0.0309 ± 0.0003	0.0310 ± 0.0003	0.0310 ± 0.0003
a	-1.218 ± 0.013	-1.214 ± 0.013	-1.214 ± 0.014	-1.213 ± 0.014
b	0.314 ± 0.023	0.310 ± 0.023	0.308 ± 0.023	0.308 ± 0.023
d	0.051 ± 0.003	0.051 ± 0.003	0.050 ± 0.003	0.050 ± 0.003
f	0.084 ± 0.019	0.082 ± 0.018	0.083 ± 0.019	0.083 ± 0.019
g	-0.039 ± 0.002	-0.039 ± 0.002	-0.039 ± 0.002	-0.039 ± 0.002
$|\mathcal{N}_n|^2$	0.256 ± 0.002	0.256 ± 0.002	0.255 ± 0.002	0.252 ± 0.008
α	-0.0242 ± 0.0049	-0.0241 ± 0.0049	-0.0247 ± 0.0048	-0.0246 ± 0.0049
β	-0.0043 ± 0.0007	-0.0043 ± 0.0008	-0.0042 ± 0.0007	-0.0042 ± 0.0007
γ	0.0013 ± 0.0004	0.0012 ± 0.0004	0.0013 ± 0.0004	0.0013 ± 0.0004

Table 5: Central results for the charged and neutral Dalitz plot parameters with isospin breaking in kinematic relations, masses in loop functions, $\pi\pi$ threshold parameters, and $\eta \to 3\pi^0$ tree level couplings (see text for details).

The modifications that arise from using physical pion masses in the loop functions and derivative couplings are very small in the expansion around the center of the Dalitz plot, see Table 5 (second column). The charged parameters are typically reduced in magnitude on the level of about 1%; α is shifted by $+0.0001$ only, an order of magnitude below the uncertainty due to different $\pi\pi$ parametrizations. The importance of pion-mass effects in loops only becomes really visible when studying the full Dalitz plot distribution also at its boundaries (see Refs. [8, 32]).

The next column in Table 5 shows the effect of isospin-breaking corrections in the $\pi\pi$ threshold parameters. For this purpose, we have calculated the electromagnetic contributions to the matching relations up-to-and-including $\mathcal{O}(e^2 p^2)$ in the chiral expansion for S- and P-wave scattering lengths and S-wave effective ranges, using the results for the one-loop $\pi\pi$ scattering amplitudes in the presence of virtual photons of Refs. [47,48]. The necessary matching procedure is described in detail in Appendix A.1. The modifications in the Dalitz plot parameters are largest for α, where a 3% effect is observed. The contributions to the remaining parameters stay well below or around 1%. In all cases the shifts are dominated by isospin-breaking corrections in the S-wave scattering lengths and thereby the $\mathcal{O}(e^2)$ chiral corrections, as expected by power counting.

Finally, we want to investigate the effects of isospin breaking on the relations in Eq. (2.11), i.e. next-to-leading order isospin breaking in the $\eta \to 3\pi$ tree level couplings. These can be extracted from the chiral one-loop calculation of the $\eta \to 3\pi$ decay amplitudes to $\mathcal{O}(e^2(m_d - m_u))$ in Ref. [8]. We write the corrections in the form

$$\mathcal{N}_n = -3\tilde{\mathcal{N}}_c + \Delta_{\tilde{\mathcal{N}}} \,, \qquad \tilde{\alpha} = \frac{1}{3}(\tilde{b} + 3\tilde{d}) + \Delta_{\tilde{\alpha}} \,, \tag{5.1}$$

where $\Delta_{\tilde{\mathcal{N}}} = \mathcal{O}(e^2(m_d - m_u))$ and $\Delta_{\tilde{\alpha}} = \mathcal{O}(e^2)$. Note that no corrections of $\mathcal{O}((m_d - m_u)^2)$

Theory	a	b	d
ChPT $\mathcal{O}(p^4)$	-1.34 ± 0.04	0.434 ± 0.018	0.077 ± 0.008
ChPT $\mathcal{O}(p^6)$	-1.271 ± 0.075	0.394 ± 0.102	0.055 ± 0.057
Dispersive	-1.16	$0.24\ldots0.26$	$0.09\ldots0.10$
$\mathcal{O}(p^4)$+NREFT	-1.213 ± 0.014	0.308 ± 0.023	0.050 ± 0.003
Experiment	a	b	d
KLOE [27]	$-1.090 \pm 0.005^{+0.008}_{-0.019}$	$0.124 \pm 0.006 \pm 0.010$	$0.057 \pm 0.006^{+0.007}_{-0.016}$
Crystal Barrel [49]	-1.22 ± 0.07	0.22 ± 0.11	0.06 ± 0.04 (input)
Layter *et al.* [50]	-1.08 ± 0.014	0.034 ± 0.027	0.046 ± 0.031
Gormley *et al.* [50]	-1.17 ± 0.02	0.21 ± 0.03	0.06 ± 0.04

Table 6: Results for the charged Dalitz plot parameters in comparison with various theoretical and experimental determinations (the next-to-leading-order errors are only due to L_3^{r}).

(in $\Delta_{\tilde{\mathcal{N}}}$) and $\mathcal{O}(m_d - m_u)$ (in $\Delta_{\tilde{\alpha}}$) occur, respectively. The analytic results of the expansion and further details are given in Appendix A.2. With the numerical input for various low-energy constants chosen as in Ref. [8], we find that the corrections to the isospin relations are very small,

$$\frac{\Delta_{\tilde{\mathcal{N}}}}{\mathcal{N}_n} = (-0.7 \pm 1.5)\% \ , \qquad \Delta_{\tilde{\alpha}} = 0.035 \pm 0.003 \ \mathrm{GeV}^{-4} \ . \tag{5.2}$$

The numerical analysis shows that the corrections to α are below 1% and thus very small, even for isospin breaking corrections. It is interesting to note that the modification induced by $\Delta_{\tilde{\alpha}}$ is largely counterbalanced by the modification due to $\Delta_{\tilde{\mathcal{N}}}$. Even though the modifications Eq. (5.1) only affect the $\eta \to 3\pi^0$ tree-level couplings, these in principle also enter the charged channel via (inelastic) rescattering effects, however these shifts are too small to register. The corresponding values, which also constitute our final results, are collected in the final column of Table 5.

After analyzing the isospin-breaking contributions we can now compare our final results for the charged Dalitz plot parameters with several other theoretical determinations and experimental findings in Table 6.

We receive mixed results for the different Dalitz plot parameters. While d is in good agreement with experiment, a shows deviations of about 10% to the results from Layter and most notably from the precision measurement of the KLOE collaboration, which – due to the relatively small errors – exceeds even very generous confidence levels. Our result is more or less compatible with the $\mathcal{O}(p^6)$ ChPT result. The dispersive calculation is somewhat closer to experiment, but no error range is given for us to compare with. The situation is even worse with b, where the deviation between our result and the KLOE measurement is rather alarming. The dispersive analysis indicates that even higher-order effects might be somewhat important in the determination of a and b, however it cannot account for the

Input	1	$\bar{a}^{\text{tree}}$	$\bar{b}^{\text{tree}}$	$\bar{d}^{\text{tree}}$
$\mathcal{N}/\tilde{\mathcal{N}}_c$	$0.9119 + 0.2954i$	$0.0028 + 0.0005i$	$-0.0097 + 0.0174i$	$-0.0156 + 0.0643i$
$\bar{a}$	$0.0202 - 0.4228i$	$1.0092 - 0.1902i$	$-0.0393 - 0.0182i$	$-0.0200 - 0.0378i$
$\bar{b}$	$-0.0421 - 0.0166i$	$0.0152 - 0.1205i$	$1.0106 - 0.0834i$	$-0.0069 + 0.0079i$
$\bar{d}$	$-0.0182 + 0.0127i$	$-0.0156 - 0.0483i$	$0.0091 - 0.0079i$	$0.9782 - 0.3583i$
$\bar{f}$	$-0.0009 - 0.0118i$	$-0.0327 + 0.0011i$	$0.0331 - 0.2371i$	$-0.0214 - 0.1175i$
$\bar{g}$	$0.0041 - 0.0027i$	$-0.0031 + 0.0074i$	$-0.0022 - 0.0115i$	$-0.0330 - 0.0783i$
$\bar{\alpha}$	$-0.0345 - 0.0028i$	$-0.0004 - 0.0964i$	$0.5823 - 0.0522i$	$0.5548 - 0.2001i$
$\bar{\beta}$	$0.0015 + 0.0028i$	$0.0090 + 0.0018i$	$-0.0108 + 0.0688i$	$-0.0036 + 0.0119i$
$\bar{\gamma}$	$-0.0010 - 0.0064i$	$-0.0008 - 0.0016i$	$-0.0216 - 0.0016i$	$-0.0075 + 0.0099i$

Table 7: Parameterization of Dalitz plot parameters in terms of tree input parameters.

discrepancy we find for b. A main source of uncertainty that we have not addressed so far is the tree-level input, which could receive rather large contributions from matching to the chiral amplitude at $\mathcal{O}(p^6)$. It is possible that the deviation in a can be accounted for by such a matching prescription. There is no indication, however, that this is also the case for b. This issue is put under tense scrutiny in the next section. The results obtained in that discussion question to some extent the consistency between the charged and neutral Dalitz plot measurements. — Our result for the cubic parameter, $f = 0.083 \pm 0.019$, is reasonably compatible with the KLOE determination, $f = 0.14 \pm 0.01 \pm 0.02$ [27].

6. Relating charged and neutral Dalitz plot parameters

6.1 Isospin limit $Q_n = Q_c$

Up to this point we have only discussed uncertainties due to the effective range parameterization in the final-state interactions. A by far greater source of uncertainty is the tree-level input to our calculation, i.e. the matching to the ChPT one-loop amplitude, which we deem responsible for most of the remaining deviation from the experimental results. At higher orders (chiral $\mathcal{O}(p^6)$), these tree parameters will receive chiral SU(3) corrections, or renormalizations of $\mathcal{O}(m_s)$, which certainly are potentially large. In order to document our findings beyond the matching to the chiral one-loop amplitude, we provide a direct parameterization of the various Dalitz plot parameters in terms of these input (tree) parameters. For this purpose, we first revert back to the case $Q_n = Q_c$ as expressions become much simpler in this limit. Table 7 shows the coefficients of the respective input parameters. The entries are to be understood as follows: e.g., the second line means that the value for $\bar{a}$ including final-state interactions is determined by the tree input according to

$$\bar{a} = 0.0202 - 0.4228i + (1.0092 - 0.1902i)\bar{a}^{\text{tree}}$$
$$- (0.0393 + 0.0182i)\bar{b}^{\text{tree}} - (0.0200 + 0.0378i)\bar{d}^{\text{tree}} \ . \tag{6.1}$$

All numerical coefficients are determined by $\pi\pi$ scattering alone. They are again averaged from the four different results (two loops plus unitarized, with ACGL and KPY parameters used as input) as in Table 4. The error range of Dalitz plot parameters calculated with this parameterization may be taken from the last column of Table 4. Furthermore, we only show the relations linear in the tree parameters (that is, no terms of quadratic etc. order), which are the by far dominant contributions.

As we will now show, Table 7 can be used to construct an explicit relation between charged and neutral channel Dalitz plot parameters. From Eq. (2.11) one can derive the following relation (again, we only consider $R_n \neq R_c$ or $Q_n \neq Q_c$ in the overall normalization for the moment):

$$\alpha = \frac{Q_n^2}{4Q_c^2}\left(d + b - |\bar{a}|^2\right) , \tag{6.2}$$

and consequently (cf. Ref. [6])

$$\alpha = \frac{Q_n^2}{4Q_c^2}\left(d + b - \frac{a^2}{4}\right) - \frac{Q_n^2}{4Q_c^2}\left(\text{Im}(\bar{a})\right)^2 \leq \frac{Q_n^2}{4Q_c^2}\left(d + b - \frac{a^2}{4}\right) , \tag{6.3}$$

which turns into an equality only for $\text{Im}(\bar{a}) = 0$. The obvious question arises: as $\text{Im}(\bar{a})$ is generated by final-state interactions but in turn depends on the Dalitz plot parameters, can we quantify the *equality* in Eq. (6.3) in such a way that we obtain a testable consistency relation between the experimental observables α, a, b, and d, *independent* of any (potentially insufficiently accurate) ChPT input? The answer is yes – precisely by using the information contained in Table 7. We consider Eq. (6.1) and first note that, to very good accuracy, the contributions from $\bar{b}^{\text{tree}}$ and $\bar{d}^{\text{tree}}$ can be neglected: with these parameters matched as previously, we have $\bar{a}^{\text{tree}} \approx -0.656$, $\bar{b}^{\text{tree}} \approx -0.017$, $\bar{d}^{\text{tree}} \approx 0.037$, which is sufficient to demonstrate that $\bar{b}^{\text{tree}}$ and $\bar{d}^{\text{tree}}$ are suppressed compared to $\bar{a}^{\text{tree}}$ by at least one order of magnitude, irrespective of potential higher-order corrections. (The neglected terms are retained explicitly in the following Sect. 6.2, compare Eq. (6.9), which fully justifies their omission.) So via $\bar{a}^{\text{tree}}$ in Eq. (6.1), $\text{Im}(\bar{a})$ can be solved for $\text{Re}(\bar{a}) = a/2$, and we find

$$\alpha = \frac{Q_n^2}{4Q_c^2}\left(b + d - \frac{a^2}{4}\right) - \zeta_1(1 + \zeta_2 a)^2 , \quad \zeta_1 = 0.050 \pm 0.005 , \quad \zeta_2 = 0.225 \pm 0.003 . \tag{6.4}$$

We wish to emphasize once more that the values for $\zeta_{1/2}$ depend solely on $\pi\pi$ rescattering effects and are independent on any chiral one-loop input. The most precise determinations of the charged Dalitz plot parameters come from the KLOE experiment [27], see Table 6. Inserting their numbers for a, b, and d into Eq. (6.4), we find

$$\alpha_{\text{KLOE,NREFT}} = -0.062 \pm 0.003(\text{stat})^{+0.004}_{-0.006}(\text{syst}) \pm 0.003(\pi\pi) , \tag{6.5}$$

where the statistical and systematic errors are calculated from the respective uncertainties and their correlations in Ref. [27], and the last error is the uncertainty inherent in our assessment of final-state interactions in Eq. (6.4). This result disagrees rather strongly with the world average of $\alpha = -0.0317 \pm 0.0016$ [42] as well as KLOE's own direct experimental finding $\alpha = -0.0301 \pm 0.0035^{+0.0022}_{-0.0035}$ [12].

This observation seems to be at odds with a result presented in Ref. [27], where a separate fit has been performed using an alternative parameterization [51], which incorporates final-state $\pi\pi$ rescattering based on a strict $\Delta I = 1$ rule and allows to extract α therefrom. The result of that alternative fit is

$$\alpha_{\Delta I=1,\mathrm{exp}} = -0.038 \pm 0.003(\mathrm{stat})^{+0.012}_{-0.008}(\mathrm{syst}) , \qquad (6.6)$$

and thus seems to be in very reasonable agreement with the direct determination of α. However, the parameterization from Ref. [51] is based on chiral one-loop phases or imaginary parts, hence leading-order rescattering with $\mathcal{O}(p^2)$ $\pi\pi$ vertices. If we reduce our rescattering formalism to that order (and also set $Q_n = Q_c$), we find for the coefficients in Eq. (6.4) $\zeta_1 = 0.021$, $\zeta_2 = 0.188$ instead, and as a result

$$\alpha_{\Delta I=1,\mathrm{NREFT}} = -0.042 \pm 0.002(\mathrm{stat})^{+0.003}_{-0.005}(\mathrm{syst}) , \qquad (6.7)$$

in satisfactory agreement with Eq. (6.6) within errors (which stem from the Dalitz plot input exclusively). We therefore understand why the rescattering formalism employed in Ref. [51] leads to a seemingly consistent result for α; however, the large impact of higher orders in the effective range parameters renders this procedure unreliable. Employing a more precise parameterization for $\pi\pi$ final-state interactions, responsible for the imaginary parts necessary for the relations Eqs. (6.3) and (6.4), shows that there seems to be a significant tension between the available experimental results for charged and neutral Dalitz plot parameters.

6.2 Isospin-breaking corrections due to $Q_n \neq Q_c$

We now study isospin-breaking corrections to the above relations due to kinematic effects stemming from $Q_n \neq Q_c$. Following the results of Sect. 5, all other effects are certainly included in the uncertainties. If we denote the charged Dalitz plot parameters as calculated in Sect. 4 by a_{iso}, b_{iso}, and so forth, the "real" ones a, b, ... as deduced from Eq. (2.9) are related to the former according to

$$
\begin{aligned}
a_{\mathrm{iso}} &= a + \delta \left(2b - a^2 \right) + \mathcal{O}(\delta^2) , \\
b_{\mathrm{iso}} &= b + \delta \left(3f - ab \right) + \mathcal{O}(\delta^2) , \\
d_{\mathrm{iso}} &= d + \delta \left(g - ad \right) + \mathcal{O}(\delta^2) ,
\end{aligned}
\qquad (6.8)
$$

where $\delta = Q_n/Q_c - 1 \approx 0.069$, and only f and g do not receive corrections as long as we disregard Dalitz plot parameters of $\mathcal{O}(\epsilon^8)$. The corrections $\propto \delta$ produce large shifts (as discussed in Sect. 5), so that one may wonder whether the relation Eq. (6.4) between charged and neutral Dalitz plot parameters may also receive large corrections. To investigate this, we have to amend Eq. (6.4) in two respects:

1. incorporate the isospin-breaking shifts due to Eq. (6.8) in the terms $b + d - a^2/4$;

2. improve the parameterization of $\mathrm{Im}(\bar{a})$ to include $\mathcal{O}(\epsilon^4)$ effects (proportional to b, d, and a^2 neglected before) in order to consistently incorporate the shifts due to Eq. (6.8) in the contribution to α stemming from the imaginary part of $\bar{a}$.

Although significantly more complicated in result, the manipulations are much the same as before, relying on Table 7. The improved result is of the form

$$\alpha = \frac{Q_n^2}{4Q_c^2}\left\{b+d-\frac{a^2}{4}-\delta\left[2a\left(b-\frac{a^2}{4}+\frac{d}{2}\right)-3f-g\right]\right\}$$
$$-\zeta_1\left[1+\zeta_2 a+\left(\zeta_3-\delta\zeta_2\right)a^2+\left(\zeta_4+2\delta\zeta_2\right)b+\zeta_5 d\right]^2, \qquad \zeta_1 = 0.050 \pm 0.005 ,$$
$$\zeta_2 = 0.223 \pm 0.003 , \quad \zeta_3 = -0.008 \pm 0.001 , \quad \zeta_4 = 0.030 \pm 0.004 , \quad \zeta_5 = 0.051 \pm 0.001 .$$
$$(6.9)$$

It turns out that the more refined description of $\mathrm{Im}(\bar{a})$ in Eq. (6.9) and therefore the complicated piece in the relation between charged and neutral Dalitz plot parameters changes the result only minimally: it shifts α by a mere $+0.001$. The term $\propto \delta$ in the first line of Eq. (6.9) is a bit more difficult to evaluate, as it involves large cancellations between the various contributions. This becomes evident, when analyzing the dependence of that term on the specific value for f. Varying f from the experimental result to our determination alone shifts the contribution of the δ-term from $+0.002$ to -0.002.

For our final result we resort to the KLOE parameters again and use correlated errors, except for g, where there is neither a measurement nor a determination of its correlation coefficients to be found in the literature. We simply choose to vary it independently between zero and the result of our calculation in Table 5. However, despite these generous variations, the total effect of these additional contributions proportional to δ is still so small that it hardly shows in the overall uncertainty. Our final result is

$$\alpha_{\mathrm{KLOE,NREFT}} = -0.059 \pm 0.003(\mathrm{stat})^{+0.004}_{-0.006}(\mathrm{syst}) \pm 0.003(\pi\pi) . \qquad (6.10)$$

The overall correction to Eq. (6.5) turns out to be small and we are still left with a significant disagreement between charged and neutral channel. Comparing the charged Dalitz plot parameters entering Eq. (6.4), we see that the main disagreement is due to the parameter b, which is strongly over-predicted in our analysis: we find $b = 0.308 \pm 0.023$ to be compared with $b_{\mathrm{KLOE}} = 0.124 \pm 0.006 \pm 0.010$. (Of course, the NREFT results are consistent within themselves: inserting our values for a, b, d into the relation Eq. (6.4) reproduces our result for α.) We also mention that there is some non-negligible variation between the KLOE results for the charged Dalitz plot parameters and several older, less precise measurements [49, 50, 52]; a re-measurement of these quantities by some of the modern high-precision experiments would therefore be very welcome.

The relation between α and the charged Dalitz plot parameters is further illustrated in Fig. 4. Due to the smallness of the higher-order corrections in Eq. (6.9), it suffices to use the simplified representation Eq. (6.4). As $\alpha = 0.0317 \pm 0.0016$ is experimentally agreed upon to very high precision, and as our result for d agrees well with the KLOE determination $d = 0.057 \pm 0.006^{+0.007}_{-0.016}$, we may take these two experimental results for granted, such that Eq. (6.4) provides a relation between a and b. This constraint in the $a-b$ plane is shown in Fig. 4. The solid grey area shows the allowed range for b as a function of a according to Eq. (6.4), whereas the hatched grey area shows the same relation for $\zeta_1 = 0$, i.e. fully neglecting the imaginary part of the amplitude, or $\mathrm{Im}(\bar{a}) = 0$. While the NREFT
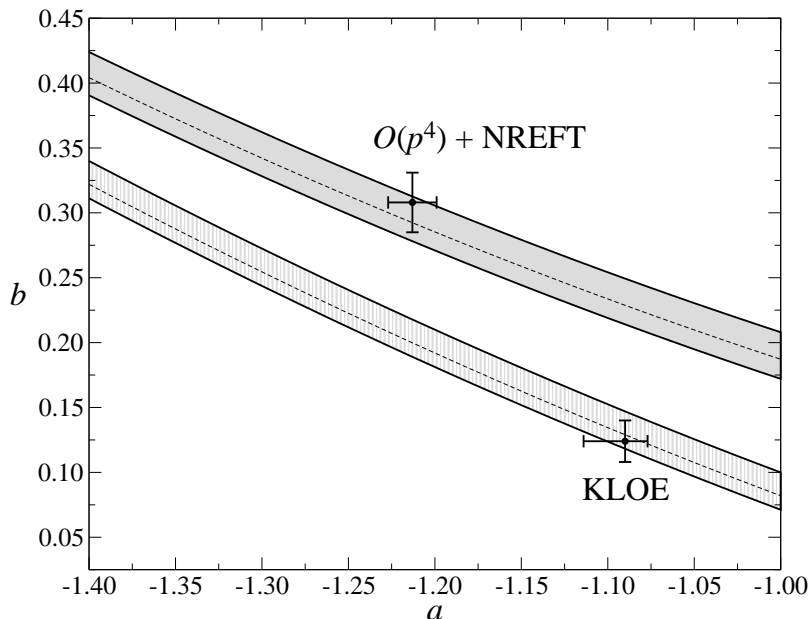
Figure 4: Allowed range for charged Dalitz plot parameters a and b with fixed α and d. Solid grey area: allowed range according to Eq. (6.4). Hatched grey area: allowed range using $\zeta_1 = 0$.

prediction for a and b falls nicely into the allowed band (the agreement here looks even better than in the direct comparison to α as the band also reflects the experimental error in d), the KLOE determination of both is consistent with a vanishing imaginary part. In our framework these latter values cannot be brought into agreement with a consistent implementation of final-state interactions.

Comparing our calculation to the dispersion-theoretical analysis of Ref. [22], there are indications that the discrepancy we find may be slightly over-predicted: in the terminology of the iterative solution determined there, our two-loop calculation cannot be expected to be better than the second iteration of the dispersive amplitude. Ref. [22] shows that while the real part of the amplitude has converged to the final result almost perfectly, there are still non-negligible corrections in the imaginary part beyond that, i.e. in terms of our representation at (irreducible) three loops and higher. Whether those corrections in the imaginary part that precisely constitute the additional terms in the relations Eqs. (6.4), (6.9) are sufficient to reduce the discrepancy between charged and neutral Dalitz plot parameter measurements remains to be seen.

7. Partial widths and the ratio r

In this work, we have concentrated almost exclusively on the energy dependence of the two $\eta \to 3\pi$ Dalitz plot distributions, mainly as encoded in the Dalitz plot parameters. It is rather obvious in particular from Table 3 that the overall *normalization* of the amplitudes is not improved in our formalism compared to what we match our parameters to, here ChPT at $\mathcal{O}(p^4)$; indeed, the overall rates are even slightly smaller. To be concrete, integrating the Dalitz plot distributions of our amplitudes including all isospin-breaking

effects (corresponding to the last column of Table 5), we find

$$\Gamma(\eta \to 3\pi^0) = \left[201 \pm 3(\pi\pi) \pm 6(\Delta_{\tilde{\mathcal{N}}})\right] \text{eV} \ ,$$
$$\Gamma(\eta \to \pi^+\pi^-\pi^0) = \left[144 \pm 2(\pi\pi)\right] \text{eV} \ . \tag{7.1}$$

Several remarks are in order here. First, as we have pointed out earlier, for our normalization we use $\mathcal{Q} = 24.2$ as given by means of Dashen's theorem, which leads to a very small width. Changing the value to $\mathcal{Q} = 22.3$ [22], say, immediately increases the widths by nearly 40%. Second, Ref. [6] finds that next-to-next-to-leading order chiral corrections increase the width by nearly 70%, thus bringing it a lot closer to the experimental value of about $\Gamma(\eta \to \pi^+\pi^-\pi^0) \approx (296 \pm 16)\,\text{eV}$ [42]. We wish to emphasize once more that this failure to reproduce the chiral enhancements in the width in the non-relativistic framework does not invalidate our predictions for the Dalitz plot parameters: the power counting argument of Sect. 3.4 explains why we catch the important rescattering effects in particular for the higher-order energy dependence, but not in the overall normalization. The $\eta \to 3\pi$ tree-level coupling constants that receive sizeable quark-mass renormalization effects nicely factor out of the complete (tree plus loop) amplitudes and play no role in the calculation of the Dalitz plot parameters. As a third remark, the errors shown in Eq. (7.1) do not at all reflect these uncertainties from our matching procedure, but purely the one due to $\pi\pi$ final-state interactions (determined as in the previous sections), and in the case of $\Gamma(\eta \to 3\pi^0)$ due to the uncertainty in $\Delta_{\tilde{\mathcal{N}}}$, see Eq. (5.1).

Despite all the above-mentioned deficits in a calculation of the decay widths, the ratio of neutral-to-charged partial widths r should be predicted much more reliably, as the normalization of the amplitude (in the isospin limit) drops out. In particular, here we may expect a somewhat heightened importance of isospin-breaking corrections [8]. We find

$$r = \frac{\Gamma(\eta \to 3\pi^0)}{\Gamma(\eta \to \pi^+\pi^-\pi^0)} = 1.40 \pm 0.01(\pi\pi) \pm 0.04(\Delta_{\tilde{\mathcal{N}}}) \ , \tag{7.2}$$

in agreement with the experimental finding $r = 1.43 \pm 0.02$ [42]. We note that the dependence on $\pi\pi$ rescattering in Eq. (7.2) is very small, our error is dominated by the 1.5% uncertainty in $\Delta_{\tilde{\mathcal{N}}}$. Equation (7.2) is extremely accurately reproduced by just integrating the phenomenological Dalitz plot distribution, with our values for the Dalitz plot parameters from Table 5 (last column) instead of the exact amplitudes: obviously r is affected by cusps in the neutral channel or yet-higher-order Dalitz plot parameters at or below the permille level. We can therefore easily derive the dependence of r on the parameters a, b, d, ..., making use of the relation of α to these in Eq. (6.3) and neglecting pieces that affect r at the permille level (e.g. the terms $\propto \beta$, γ in the neutral rate), and find

$$r = 1.485 \left(1 - 0.029\,a - 0.061\,a^2 + 0.024\,b + 0.032\,d + 0.008\,f - 0.014\,g\right) \left(1 + \frac{2\Delta_{\tilde{\mathcal{N}}}}{\mathcal{N}_n}\right) \ . \tag{7.3}$$

Errors on this result are to be taken from Eq. (7.2). The various numerical coefficients are given by $\pi\pi$ phase shifts and phase space integration only. This demonstrates to very good approximation that r does not depend on the normalization and thus possibly sizeable quark mass renormalization effects.

8. Summary and conclusion

In this article we have analyzed rescattering effects in $\eta \to 3\pi$ decays by means of the modified non-relativistic effective field theory framework. The main findings of our investigation can be summarized as follows:

1. NREFT provides a simple and transparent representation of the amplitude to two loops, including higher-order isospin breaking. In order to estimate higher-order loop effects we have furthermore applied a simplified unitarization prescription. The amplitude thus obtained is – at the very least – fully competitive with the chiral expansion at next-to-next-to-leading order. The coupling constants involved have been matched to phenomenological $\pi\pi$ scattering threshold parameters and, in the case of the $\eta \to 3\pi$ tree-level couplings, to ChPT at $\mathcal{O}(p^4)$.

2. One- and two-loop contributions to the Dalitz plot parameters are in general of the same size, an observation which is predicted by non-relativistic power counting arguments. Irreducible two-loop graphs are generally suppressed, while derivative couplings at two-loop level are essential to find the correct sign for the $\eta \to 3\pi^0$ slope parameter α. Higher-order effects beyond two loops were shown to be relatively small, but not negligible.

3. While our results for the Dalitz plot parameters are in qualitative agreement with previous dispersive results, we can provide an explanation for the apparent failure of two-loop ChPT to reproduce α: the treatment of $\pi\pi$ final-state interactions is still not sufficiently accurate at that order. We can identify one specific diagram, the double rescattering graph with $\pi\pi$ vertices beyond leading order, as being responsible for at least half of the discrepancy between the $\mathcal{O}(p^6)$ prediction for α and the experimental value. These effects are of chiral order p^8 and higher, but included in the NREFT two-loop representation.

4. Apart from normalization effects and subtleties in the definition of the center of the Dalitz plot in the charged decay channel, higher-order isospin-breaking corrections on the Dalitz plot parameters are very small.

5. Our final result for neutral Dalitz slope parameter,

$$\alpha = -0.025 \pm 0.005 \ , \tag{8.1}$$

is compared in Fig. 5 to several other determinations. It is considerably closer to the experimental world average $\alpha = -0.0317 \pm 0.0016$ [42] than previous theoretical approaches. Notice though that Eq. (8.1) does not take uncertainties stemming from matching to ChPT at $\mathcal{O}(p^4)$ into account, which we expect to be non-negligible.

6. Our results for the charged Dalitz plot parameters show somewhat larger deviations from the currently most accurate measurement by the KLOE collaboration. By relating charged and neutral decay channel via the $\Delta I = 1$ rule we find indications
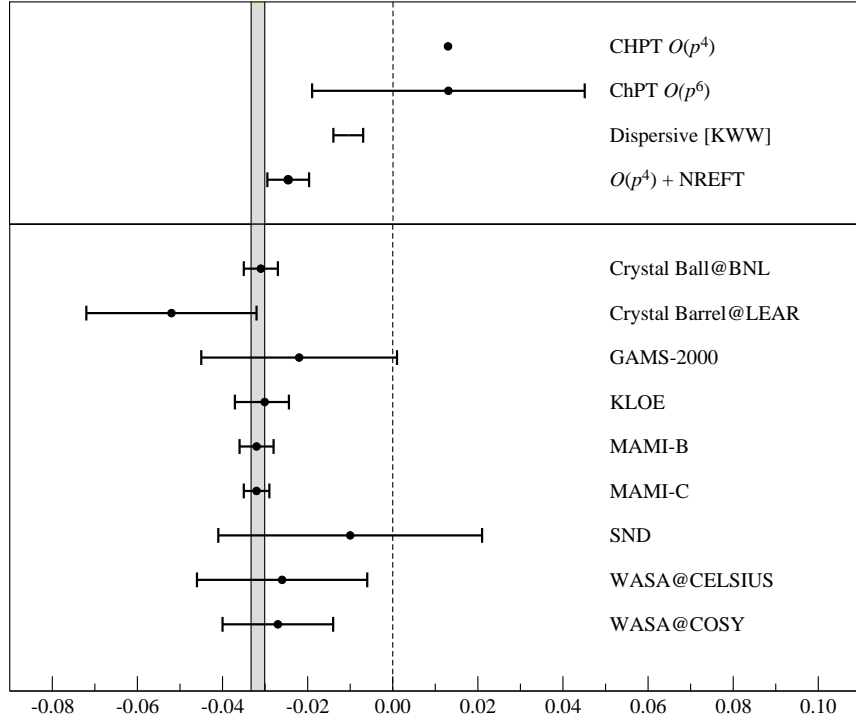
Figure 5: Comparison of values for the slope parameter α. Top: theoretical predictions. Bottom: experimental determinations. The grey shaded area is the particle data group average [42].

for a significant tension between the Dalitz plot parameters of both channels, which is solely due to final-state interactions. A re-measurement of the charged Dalitz plot parameters by high-precision experiments [53, 54], or even preferably access to improved full Dalitz plot distributions, is thus highly desirable.

7. While the partial widths calculated in our framework do not improve upon the chiral one-loop prediction we match to (due to the absence of further quark-mass renormalization effects not captured in our framework), we can give a value for the ratio of neutral-to-charged partial widths unaffected by this deficit, $r = 1.40 \pm 0.04$, where the error is dominated by isospin-breaking effects.

Possible future improvements on the theoretical approach include matching to $\mathcal{O}(p^6)$ ChPT in order to constrain the tree-level Dalitz plot couplings more tightly. Furthermore, it will be extremely useful to match the non-relativistic representation to the upcoming dispersive analysis [22] in order to obtain a reliable description of the whole physical Dalitz plot: in this way one can include elastic $\pi\pi$ rescattering to all orders, and at the same time implement in particular non-analytic effects (cusps) at or near the boundaries of the Dalitz plot due to isospin-breaking up to next-to-next-to-leading order. This combination should then also provide the best-possible representation of the decay amplitude for a precision extraction of the quark mass ratio $\mathcal{Q}$.

Acknowledgements

We would like to thank Gilberto Colangelo, Jürg Gasser, Andrzej Kupść, Stefan Lanz, and Akaki Rusetsky for stimulating discussions, and Jürg Gasser for numerous useful remarks on the manuscript.

A. Isospin-breaking corrections

A.1 Isospin-breaking corrections to $\pi\pi$ scattering

To calculate isospin-breaking corrections to the matching relations Eq. (3.7), we expand the ChPT amplitudes for all channels with electromagnetic corrections included [47, 48] around threshold. These contain virtual-photon exchange and real-photon radiation in the form of bremsstrahlung. For the definition of a reasonable (regular) threshold expansion, at first the divergent Coulomb pole contribution has to be subtracted. As the Coulomb pole emerges equally in the vertex correction diagram in both the NREFT and the ChPT calculation due to the same infrared properties of both theories, in a matching between them, this part drops out anyway. The determination of the scattering lengths is then relatively straightforward and has already been performed in the above references. Note, however, that in contrast to Refs. [47, 48] we expand around an isospin limit defined in terms of the *charged* pion mass. Thus, non-analytic terms $\propto \sqrt{\Delta_\pi}$ arise in the expansion of the $\pi^0\pi^0 \to \pi^0\pi^0$ channel, which are due to a cusp structure at the charged pion threshold and cancel the corresponding contribution in the expansion of $J_{+-}(s)$ in Eq. (3.3), once the correct matching is performed. We display the corrections in the form $C_i = \bar{C}_i + \Delta C_i$, where $\bar{C}_i$ denotes the corresponding coupling in the isospin limit (the $\pi^+\pi^+ \to \pi^+\pi^+$ channel is not needed in the present analysis, we just give it for completeness). For the combinations of S-wave scattering lengths, we find

$$\Delta C_{00} = \frac{M_\pi^2}{F_\pi^2}\left\{-\frac{\Delta_\pi}{M_\pi^2} + \frac{e^2}{32\pi^2}\mathcal{K}^{00} + \frac{\Delta_\pi}{32\pi^2 F_\pi^2}\left(13 - 16\bar{l}_1 - 32\bar{l}_2 + 6\bar{l}_3 - 4\bar{l}_4\right)\right\},$$

$$\Delta C_x = \frac{M_\pi^2}{F_\pi^2}\left\{-\frac{\Delta_\pi}{M_\pi^2} + \frac{e^2}{32\pi^2}\left(30 - 3\mathcal{K}_1^{\pm 0} + \mathcal{K}_2^{\pm 0}\right) - \frac{\Delta_\pi}{96\pi^2 F_\pi^2}\left(23 + 8\bar{l}_1 + 6\bar{l}_3 + 12\bar{l}_4\right)\right\},$$

$$\Delta C_{+0} = \frac{M_\pi^2}{F_\pi^2}\left\{\frac{\Delta_\pi}{M_\pi^2} - \frac{e^2}{32\pi^2}\left(2 + \mathcal{K}_1^{\pm 0} + \mathcal{K}_2^{\pm 0}\right) + \frac{\Delta_\pi}{96\pi^2 F_\pi^2}\left(3 - 8\bar{l}_1 - 16\bar{l}_2 + 6\bar{l}_3 + 12\bar{l}_4\right)\right\},$$

$$\Delta C_{+-} = \frac{M_\pi^2}{F_\pi^2}\left\{\frac{2\Delta_\pi}{M_\pi^2} - \frac{e^2}{16\pi^2}\left(24 - \mathcal{K}^{+-}\right) + \frac{\Delta_\pi}{8\pi^2 F_\pi^2}\left(2 + \bar{l}_3 + 2\bar{l}_4\right)\right\},$$

$$\Delta C_{++} = \frac{M_\pi^2}{F_\pi^2}\left\{\frac{2\Delta_\pi}{M_\pi^2} - \frac{e^2}{16\pi^2}\left(20 - \mathcal{K}^{++}\right) + \frac{\Delta_\pi}{16\pi^2 F_\pi^2}\left(3 + 2\bar{l}_3 + 4\bar{l}_4\right)\right\}. \tag{A.1}$$

We note that ΔC_{00} is indeed free of non-analytic terms in Δ_π: the analytic structure of ChPT and the non-relativistic representation near threshold is the same, as it must.

The definition of effective ranges and P-wave scattering lengths is not *a priori* clear, since one has to deal with infrared divergences in the ChPT amplitudes. In calculations of, say, cross sections these divergences, which arise from virtual-photon corrections, cancel with corresponding divergences from real-photon radiation (bremsstrahlung). However, when matching the non-relativistic framework to ChPT, the explicit inclusion of

bremsstrahlung is not necessary, since the virtual-photon diagrams exhibit the same infrared behavior and thus contain the same divergences (see Ref. [31]). On a rather technical note, the infrared divergences were calculated in dimensional regularization in Ref. [31], while the ChPT calculations [47, 48] use a finite photon mass m_γ as infrared regulator. The transition between both regularization schemes can be made by replacing $\log(m_\gamma^2/M_\pi^2) \to -32\pi^2\lambda_{\mathrm{IR}} - 1$. The infrared divergences then cancel, rendering the matching relations finite. We wish to emphasize that the physical reason for this cancellation is again the identical infrared behavior of both theories.

For the S-wave effective ranges, defining in analogy with the above $D_i = \bar{D}_i + \Delta D_i$, we find the following corrections to the matching relations:

$$\Delta D_{00} = \frac{1}{F_\pi^2}\left\{\frac{\Delta_\pi}{48\pi^2 F_\pi^2}\big(35 - 8\bar{l}_1 - 16\bar{l}_2\big)\right\} ,$$

$$\Delta D_x = \frac{1}{F_\pi^2}\left\{\frac{e^2}{96\pi^2}\big(59 - 3\mathcal{K}_1^{\pm 0}\big) + \frac{\Delta_\pi}{120\pi^2 F_\pi^2}\big(18 - 5\bar{l}_1\big)\right\} ,$$

$$\Delta D_{+0} = \frac{1}{F_\pi^2}\left\{-\frac{e^2}{192\pi^2}\big(1 + 3\mathcal{K}_1^{\pm 0}\big) + \frac{\Delta_\pi}{192\pi^2 F_\pi^2}\big(21 - 4\bar{l}_1 - 12\bar{l}_2\big)\right\} ,$$

$$\Delta D_{+-} = \frac{1}{F_\pi^2}\left\{-\frac{e^2}{1152\pi^2}\Big(764 - 9(\mathcal{K}^{+-} - \mathcal{K}^{++})\Big) - \frac{109\Delta_\pi}{384\pi^2 F_\pi^2}\right\} ,$$

$$\Delta D_{++} = \frac{1}{F_\pi^2}\left\{-\frac{e^2}{576\pi^2}\Big(676 + 9(\mathcal{K}^{+-} - \mathcal{K}^{++})\Big) + \frac{61\Delta_\pi}{192\pi^2 F_\pi^4}\right\} , \tag{A.2}$$

while for the two P-wave scattering lengths, we have (with $E_i = \bar{E}_i + \Delta E_i$)

$$\Delta E_{+0} = \frac{1}{F_\pi^2}\left\{\frac{e^2}{64\pi^2}\big(1 + 3\mathcal{K}_1^{\pm 0}\big) - \frac{\Delta_\pi}{192\pi^2 F_\pi^2}\big(19 - 12\bar{l}_1 + 12\bar{l}_2\big)\right\} ,$$

$$\Delta E_{+-} = \frac{1}{F_\pi^2}\left\{\frac{3e^2}{128\pi^2}\big(-28 + \mathcal{K}^{+-} - \mathcal{K}^{++}\big) - \frac{93\Delta_\pi}{128\pi^2 F_\pi^2}\right\} , \tag{A.3}$$

where the following abbreviations have been used for combinations of electromagnetic SU(2) low-energy constants $\bar{k}_i$ and $Z = \Delta_\pi/(2e^2 F_\pi^2)$:

$$\mathcal{K}^{00} = \Big(3 + \frac{4Z}{9}\Big)\bar{k}_1 - \frac{40Z}{9}\bar{k}_2 - 3\bar{k}_3 - 4Z\bar{k}_4 ,$$

$$\mathcal{K}_1^{\pm 0} = \Big(3 + \frac{4Z}{9}\Big)\bar{k}_1 + \frac{32Z}{9}\bar{k}_2 + 3\bar{k}_3 + 4Z\bar{k}_4 ,$$

$$\mathcal{K}_2^{\pm 0} = 8Z k_2 + 3\bar{k}_3 + 4Z\bar{k}_4 - 2(1 + 8Z)\bar{k}_6 - (1 - 8Z)\bar{k}_8 ,$$

$$\mathcal{K}^{+-} = \Big(3 + \frac{4Z}{9}\Big)\bar{k}_1 - \frac{40Z}{9}\bar{k}_2 - 9\bar{k}_3 + 4Z\bar{k}_4 + 4(1 + 8Z)\bar{k}_6 + 2(1 - 8Z)\bar{k}_8 ,$$

$$\mathcal{K}^{+-} - \mathcal{K}^{++} = 2\Big(3 + \frac{4Z}{9}\Big)\bar{k}_1 + \frac{208Z\bar{k}_2}{9} - 18\bar{k}_3 + 24Z\bar{k}_4 . \tag{A.4}$$

We refrain from calculating corrections to the shape parameters, since their intrinsic, isospin-symmetric error is much larger than what can be expected from isospin breaking.

For the numerical evaluation we express the low-energy constants $\bar{l}_1$ and $\bar{l}_2$ in terms of $\pi\pi$ D-wave scattering lengths [55], for which we use the numerical values [39]

$$a_2^0 = 1.75 \pm 0.03 \times 10^{-3} M_\pi^{-4} , \qquad a_2^2 = 0.170 \pm 0.013 \times 10^{-3} M_\pi^{-4} . \tag{A.5}$$

channel	$\Delta C_i/C_i \times 10^{-2}$	$\Delta D_i/D_i \times 10^{-2}$	$\Delta E_i/E_i \times 10^{-2}$
00	-7.3 ± 0.2	-3.3 ± 0.4	–
x	2.5 ± 0.6	0.1 ± 0.6	–
+0	-5.2 ± 0.8	1.9 ± 0.8	0.4 ± 0.6
+−	6.1 ± 0.5	-0.2 ± 0.3	0.5 ± 0.4

Table 8: Corrections to the matching relations relative to the phenomenological values.

This way a_2^0 and a_2^2 can be independently varied according to their uncertainty, whereas $\bar{l}_1$ and $\bar{l}_2$ are correlated. For $\bar{l}_3$ we propose $\bar{l}_3 = 3.1 \pm 0.5$ as a sensible mean value from lattice simulations (see Ref. [56] for individual results of the various groups). The constant $\bar{l}_4$ is extracted from the scalar radius of the pion [39], $\bar{l}_4 = 4.4 \pm 0.2$.

For the electromagnetic SU(2) low-energy constants k_i^r we use the values given in Ref. [57]. The authors of this work have matched the two-flavor low-energy constants to their SU(3) counterparts, using numerical estimates from Refs. [58, 59]. We convert the values k_i^r given at the mass of the ρ, $M_\rho = 0.77$ GeV, in Ref. [57] to scale-independent constants according to the standard prescription,

$$\bar{k}_i = \frac{32\pi^2}{\sigma_i} k_i^r(M_\rho) - \log \frac{M_\pi^2}{M_\rho^2} , \tag{A.6}$$

where the σ_i are the corresponding β-functions to be found in Ref. [47]. Numerically this results in

$$\bar{k}_1 = 1.66 , \quad \bar{k}_2 = 4.08 , \quad \bar{k}_3 = 2.28 , \quad \bar{k}_4 = 3.69 , \quad \bar{k}_6 = 4.08 , \quad \bar{k}_8 = 4.06 . \tag{A.7}$$

The uncertainties on the k_i^r are estimated analogously to Ref. [8] by their logarithmic scale variation,

$$k_i^r \to k_i^r \pm \frac{\sigma_i}{16\pi^2} , \tag{A.8}$$

which for the $\bar{k}_i$ translates to $\bar{k}_i \to \bar{k}_i \pm 2$. The errors on the quantities $\mathcal{K}^{00}, \mathcal{K}_i^{\pm 0}, \mathcal{K}^{+-}, \mathcal{K}^{++}$ are then calculated in a correlated fashion (i.e. $+2$ or -2 for *all* $\bar{k}_i$).

The numerical corrections are displayed in Table 8. We find that the corrections at one-loop order are very small. The main contributions to the C_i stem from the tree-level correction factor.

A.2 Corrections to the $\Delta I = 1$ rule

At leading order p^2 in ChPT and up to next-to-leading order in the isospin-breaking parameters $m_u - m_d$ and e^2, the amplitudes for the charged and the neutral decay were already quoted in Eq. (2.6). We also hinted at the fact that in order to define the deviations from the $\Delta I = 1$ relation, Eq. (5.1), it is useful to expand the decay amplitudes for *both* channels around the point $s_3 = s_n$, $s_1 = s_2$ as shown in Eq. (2.8), so that $\Delta_{\tilde{\mathcal{N}}}$ is going to be of chiral order p^4.

The decay amplitudes at $\mathcal{O}(p^4)$ in ChPT and at $\mathcal{O}(m_d - m_u, e^2, (m_d - m_u)e^2)$ in isospin breaking are given explicitly in Ref. [8]. With minimal modifications they can be shown to be also valid up-to-and-including $\mathcal{O}((m_d - m_u)^2)$, i.e. only numerically tiny terms of $\mathcal{O}(e^4)$ are potentially neglected at second order in isospin breaking. In order to match the expanded ChPT amplitude of Ref. [8] to the polynomial part of the NREFT representation, the following steps have to be taken into account:

1. The (non-analytic) imaginary parts due to pion loops in chiral and NREFT amplitude are identical and drop out in the matching relation.

2. For the radiative corrections due to real and virtual photons, we have to match the result of Ref. [8] to an analogous NREFT representation as in Ref. [31]. As a result, the Coulomb pole and phase have to be subtracted from the chiral representation, as well as the bremsstrahlung contributions. As in the case of radiative corrections to $\pi\pi$ scattering infrared divergences were regulated by introducing a finite photon mass m_γ in Ref. [8] and have to be treated as described in Appendix A.1.

As $\Delta_{\tilde{\mathcal{N}}}$ is of $\mathcal{O}(p^4)$, it is convenient to factor out the neutral normalization at leading order and quote the result as the ratio $\Delta_{\tilde{\mathcal{N}}}/\mathcal{N}_n$ below. We find

$$
\begin{aligned}
\frac{\Delta_{\tilde{\mathcal{N}}}}{\mathcal{N}_n} &= 2e^2 \left\{ \frac{1-3\rho}{3\rho} G(s_n) + \frac{1}{2}\bar{J}_{\pi\pi}(s_n) + \frac{3}{32\pi^2}\left(\log\frac{M_\pi^2}{\mu^2} - 1 \right) - \frac{1+\rho}{1-\rho}(2K_3^r - K_4^r) \right.\\
&\left. \quad + \frac{8K_6^r}{3(1-\rho)} - \frac{4(3-\rho)}{1-\rho}(K_{10}^r + K_{11}^r) \right\}\\
&+ \frac{\Delta_\pi}{3(1-\rho)F_\pi^2}\left\{ \frac{29 - 111\rho - 9\rho^2 + 27\rho^3}{8(1+3\rho)}\bar{J}_{KK}(s_n) - 32L_3^r \right.\\
&\quad + \frac{3\rho(1 + 22\rho + 9\rho^2)}{(1-9\rho)(1+3\rho)}\bar{J}_{\eta\pi}(s_n) - \frac{7 + 21\rho - 495\rho^2 + 243\rho^3}{(1-9\rho)(1+3\rho)}\bar{J}_{\pi\pi}(s_n)\\
&\quad + \frac{8(3-\rho)}{1-\rho}\frac{F_\pi^2}{M_\eta^2}\Delta_F + \frac{1}{16\pi^2}\left[6(3 - 2\rho)\log\frac{M_\pi^2}{\mu^2} + \frac{2(1 + 2\rho - \rho^2)}{1-\rho}\log\frac{3+\rho}{4\rho} \right.\\
&\left.\left. \quad - \frac{3(3 - 26\rho - \rho^2)}{(1-9\rho)(1-\rho)}\log\rho + \frac{53 - 357\rho + 351\rho^2 + 81\rho^3}{4(1-9\rho)} \right] \right\} + \mathcal{O}\left(e^2 p^2\right),\quad \text{(A.9)}\\
\Delta_{\tilde{\alpha}} &= \frac{3e^2}{(1-9\rho)^2(1-\rho)(1+3\rho)^2 M_\eta^4}\left\{ 12\rho(1 + 63\rho^2)G(s_n) \right.\\
&\quad - \frac{1 - 14\rho - 138\rho^2 + 234\rho^3 - 1107\rho^4}{1-9\rho}\bar{J}_{\pi\pi}(s_n)\\
&\left. \quad + \frac{7 - 102\rho - 504\rho^2 + 1926\rho^3 - 3375\rho^4}{32\pi^2(1-9\rho)} \right\}\\
&+ \frac{3\Delta_\pi}{(1-\rho)(1+3\rho)^2 F_\pi^2 M_\eta^4}\left\{ \frac{3(3+\rho)(957 - 5240\rho - 1398\rho^2 - 288\rho^3 + 81\rho^4)}{4096(1+3\rho)}\bar{J}_{KK}(s_n) \right.\\
&\quad + \frac{\rho^2(221 - 3612\rho + 32022\rho^2 - 32076\rho^3 - 2187\rho^4)}{8(1-9\rho)^3(1+3\rho)}\bar{J}_{\eta\pi}(s_n)\\
&\left. \quad - \frac{3\rho(3 - 124\rho + 1794\rho^2 - 7596\rho^3 + 9315\rho^4)}{(1-9\rho)^3(1+3\rho)}\bar{J}_{\pi\pi}(s_n) \right.
\end{aligned}
$$

$$+ \frac{1}{32768\pi^2(1-9\rho)^3}\Big(243 - 39737\rho + 540471\rho^2 - 729333\rho^3$$

$$+ 3630825\rho^4 - 1810107\rho^5 + 85293\rho^6 + 59049\rho^7\Big)$$

$$- \frac{\rho^2(37 + 237\rho - 2025\rho^2 + 3159\rho^3)}{128\pi^2(1-9\rho)^3(1-\rho)}\log\rho\Big\} + \mathcal{O}\left(e^2 p^{-2}\right) , \tag{A.10}$$

neglecting even higher-order terms in the isospin-breaking parameters e^2 and $m_d - m_u$. Here, we have used $\Delta_F = F_K/F_\pi - 1$ (cf. Ref. [60]) and the loop functions

$$G(s) = \frac{1-\sigma_\pi^2}{64\pi^2\sigma_\pi}\left\{ \mathrm{Li}\left(\frac{1-\sigma_\pi}{1+\sigma_\pi}\right) - \mathrm{Li}\left(\frac{1+\sigma_\pi}{1-\sigma_\pi}\right) + \log\frac{1+\sigma_\pi}{1-\sigma_\pi}\right\} , \quad \mathrm{Li}(z) = \int_1^z \frac{\log t}{1-t}dt ,$$

$$\bar{J}_{\pi\pi}(s) = \frac{1}{8\pi^2}\left\{1 - \frac{\sigma_\pi}{2}\log\frac{1+\sigma_\pi}{1-\sigma_\pi}\right\} , \qquad \bar{J}_{KK}(s) = \frac{1}{8\pi^2}\left\{1 - \sigma_K \,\mathrm{arccot}\,\sigma_K\right\} ,$$

$$\bar{J}_{\eta\pi}(s) = \frac{1}{32\pi^2}\left\{2 + \log\rho\left(\frac{M_\eta^2 - M_\pi^2}{s} - \frac{1+\rho}{1-\rho}\right) - \frac{\nu}{s}\log\frac{s - M_\eta^2 - M_\pi^2 + \nu}{s - M_\eta^2 - M_\pi^2 + \nu}\right\} ,$$

$$\sigma_\pi = \sqrt{1 - \frac{4M_\pi^2}{s}} , \quad \sigma_K = \sqrt{\frac{4M_K^2}{s} - 1} , \quad \nu = \lambda^{1/2}(M_\eta^2, M_\pi^2, s) , \quad \rho = \frac{M_\pi^2}{M_\eta^2} . \tag{A.11}$$

$G(s)$ is the real part of the triangle loop function for the photon exchange between two charged pions (rescaled by a factor of M_π^2) with the Coulomb pole subtracted, involving Spence's function $\mathrm{Li}(z)$, and $\bar{J}_{ab}(s)$ are the usual finite and scale-independent parts of the corresponding two-meson loop functions. For the definition of the (renormalized) strong and electromagnetic SU(3) low-energy constants L_3^r and K_i^r in terms of chiral Lagrangians (not to be confused with the tree-level couplings L_i, K_i of the non-relativistic theory), see Refs. [60, 61]. We have made extensive use of the Gell-Mann–Okubo relation to simplify the results Eqs. (A.9) and (A.10). Furthermore, the kinematic expansion to second order plus the expansion in isospin-breaking parameters leads to derivatives up to third order of these loop functions, which have been rewritten in terms of the loop functions themselves.

Both results Eqs. (A.9) and (A.10) are divergence-free and independent of the scale μ. The scale-independence of $\Delta_{\tilde\alpha}$ is explicitly seen, that of $\Delta_{\tilde{\mathcal{N}}}$ can be found by using the scale variation of the electromagnetic constants K_i^r as given in Ref. [61]. Both corrections turn out to be completely of electromagnetic origin. For the numerical evaluation we make use of the same estimates and variations of the low-energy constants as described in Appendix A.1 and explained in more detail in Ref. [8]; their uncertainties completely dominate the error on $\Delta_{\tilde{\mathcal{N}}}/\mathcal{N}_n$. As $\Delta_{\tilde\alpha}$ is free of low-energy constants at this order, it is a pure loop effect and a prediction in terms of well-known parameters. Here we quote an uncertainty solely due to the use of the Gell-Mann–Okubo relation for the masses, using either the mass of the η directly, or the same expressed in terms of pion and kaon masses. We consider the error thus obtained rather underestimated. In total, we find

$$\frac{\Delta_{\tilde{\mathcal{N}}}}{\mathcal{N}_n} = (-0.7 \pm 1.5)\% , \qquad \Delta_{\tilde\alpha} = 0.035 \pm 0.003 \text{ GeV}^{-4} . \tag{A.12}$$

B. NREFT representation including isospin breaking

B.1 $\eta \to 3\pi$ amplitudes up to two loops

For the representation of the $\eta \to 3\pi$ decay amplitudes at one-loop order, we find (see also Ref. [30])

$$\mathcal{M}_n^{\text{1-loop}}(s_1, s_2, s_3) = \Big\{ C_{00}(s_1) K(s_1) J_{00}(s_1) + 2 C_x(s_1) L(s_1) J_{+-}(s_1) + (s_1 \leftrightarrow s_2)$$
$$+ (s_1 \leftrightarrow s_3) \Big\} \,,$$

$$\mathcal{M}_c^{\text{1-loop}}(s_1, s_2, s_3) = C_x(s_3) K(s_3) J_{00}(s_3) + 2 C_{+-}(s_3) L(s_3) J_{+-}(s_3)$$
$$+ \Big\{ \Big[2 C_{+0}(s_1) L'(s_1) - \tilde{E}_{+0}(s_1, s_2, s_3) \tilde{L}(s_1) \Big] J_{+0}(s_1) + (s_1 \leftrightarrow s_2) \Big\} \,. \quad \text{(B.1)}$$

The topologies at two-loop order are shown in Fig. 2. For the two-loop amplitudes at the order discussed in Sect. 3.4, we obtain

$$\mathcal{M}_n^{\text{2-loops}} = \Big\{ \mathcal{M}_n^A(s_1, s_2, s_3) + \mathcal{M}_n^B(s_1, s_2, s_3) + (s_1 \leftrightarrow s_2) + (s_1 \leftrightarrow s_3) \Big\} \,,$$
$$\mathcal{M}_c^{\text{2-loops}} = \mathcal{M}_c^A(s_1, s_2, s_3) + \mathcal{M}_n^B(s_1, s_2, s_3) \,, \quad \text{(B.2)}$$

where

$$\mathcal{M}_n^A = 2 K_0 C_{00}(\tilde{s}_1^{00}) C_{00}(s_1) F_0(M_{\pi^0}, M_{\pi^0}, M_{\pi^0}, M_{\pi^0}, s_1)$$
$$- 4 M_\eta K_0 D_{00} C_{00}(s_1) \frac{\mathbf{Q}_1^2}{Q_1^0} F_0^{(1)}(M_{\pi^0}, M_{\pi^0}, M_{\pi^0}, M_{\pi^0}, s_1)$$
$$+ 8 \Big[L'''_{+0}(s_1) C_{+0}(\tilde{s}_1^{+-})$$
$$- \frac{\Delta_\pi}{4 M_{\pi^0}} \Big(\frac{s_1 + 2 \mathbf{Q}_1^2}{2 Q_1^0} - p_1^0 \Big) L_0 E_{+0} \Big] C_x(s_1) F_0(M_{\pi^0}, M_\pi, M_\pi, M_\pi, s_1)$$
$$- 8 \Big[\frac{1}{2} L_1 C_{+0}(\tilde{s}_1^{+-}) + 2 M_\eta L'''_{+0}(s_1) D_{+0}$$
$$- \frac{\Delta_\pi}{4 M_{\pi^0}} L_0 E_{+0} \Big] C_x(s_1) \frac{\mathbf{Q}_1^2}{Q_1^0} F_0^{(1)}(M_{\pi^0}, M_\pi, M_\pi, M_\pi, s_1)$$
$$+ 8 M_\eta L_1 D_{+0} C_x(s_1) \frac{\mathbf{Q}_1^4}{(Q_1^0)^2} F_0^{(2)}(M_{\pi^0}, M_\pi, M_\pi, M_\pi, s_1)$$
$$+ 4 L''(s_1) C_x(\tilde{s}_1^{00}) C_{00}(s_1) F_0(M_\pi, M_\pi, M_{\pi^0}, M_{\pi^0}, s_1)$$
$$+ 4 \Big[L_1 C_x(\tilde{s}_1^{00}) - 2 M_\eta L''(s_1) D_x \Big] C_{00}(s_1) \frac{\mathbf{Q}_1^2}{Q_1^0} F_0^{(1)}(M_\pi, M_\pi, M_{\pi^0}, M_{\pi^0}, s_1)$$
$$- 8 M_\eta L_1 D_x C_{00}(s_1) \frac{\mathbf{Q}_1^4}{(Q_1^0)^2} F_0^{(2)}(M_\pi, M_\pi, M_{\pi^0}, M_{\pi^0}, s_1) \,, \quad \text{(B.3)}$$

$$\mathcal{M}_n^B = K(s_1) C_{00}(s_1)^2 J_{00}^2(s_1) + 2 \Big[L(s_1) C_x(s_1) C_{00}(s_1) + K(s_1) C_x^2(s_1) \Big] J_{00}(s_1) J_{+-}(s_1)$$
$$+ 4 L(s_1) C_{+-}(s_1) C_x(s_1) J_{+-}^2(s_1) \,, \quad \text{(B.4)}$$

$$\mathcal{M}_c^A = \Big\{ 4 \Big[L'''_{+0}(s_1^+) C_{+0}(\tilde{s}_1^{+0}) \Big(C_{+0}(s_1) - E_{+0}^+(s_1, s_2, s_3) \Big)$$

– 38 –

$$+ \frac{\Delta_\pi}{4M_{\pi^0}}\Big(\frac{s_1 + 2\mathbf{Q}_1^2 - \Delta_\pi}{2Q_1^0} - p_1^0\Big)L_0 E_{+0}C_{+0}(s_1)\Big]F_+(M_\pi, M_{\pi^0}, M_\pi, M_{\pi^0}, s_1)$$

$$- 4\Big[\Big(\frac{1}{2}L_1 C_{+0}(\tilde{s}_1^{+0}) + 2M_\eta L_{+0}'''(s_1^+)D_{+0}\Big)\Big(C_{+0}(s_1) - E_{+0}^+(s_1, s_2, s_3)\Big)\frac{\mathbf{Q}_1^2}{Q_1^0}$$

$$+ \frac{\Delta_\pi}{4M_{\pi^0}}L_0 E_{+0}C_{+0}(s_1)\frac{\mathbf{Q}_1^2}{Q_1^0}$$

$$- 2L_{+0}'''(s_1^+)C_{+0}(\tilde{s}_1^{+0})E_{+0}(s_1, s_2, s_3)\Big]F_+^{(1)}(M_\pi, M_{\pi^0}, M_\pi, M_{\pi^0}, s_1)$$

$$+ 4\Big[M_\eta L_1 D_{+0}\Big(C_{+0}(s_1) - E_{+0}^+(s_1, s_2, s_3)\Big)\frac{\mathbf{Q}_1^4}{(Q_1^0)^2} - \Big(L_1 C_{+0}(\tilde{s}_1^{+0})$$

$$+ 4M_\eta L_{+0}'''(s_1^+)D_{+0}\Big)E_{+0}(s_1, s_2, s_3)\frac{\mathbf{Q}_1^2}{Q_1^0}\Big]F_+^{(2)}(M_\pi, M_{\pi^0}, M_\pi, M_{\pi^0}, s_1)$$

$$+ 8M_\eta L_1 D_{+0}E_{+0}(s_1, s_2, s_3)\frac{\mathbf{Q}_1^4}{(Q_1^0)^2}F_+^{(3)}(M_\pi, M_{\pi^0}, M_\pi, M_{\pi^0}, s_1)$$

$$+ 4L''(s_1^-)C_{+-}(\tilde{s}_1^{0+})\Big(C_{+0}(s_1) + E_{+0}^-(s_1, s_2, s_3)\Big)F_+(M_\pi, M_\pi, M_{\pi^0}, M_\pi, s_1)$$

$$+ 4\Big[\Big(L_1 C_{+-}(\tilde{s}_1^{0+}) - 2M_\eta L''(s_1^-)D_{+-}\Big)\Big(C_{+0}(s_1) + E_{+0}^-(s_1, s_2, s_3)\Big)\frac{\mathbf{Q}_1^2}{Q_1^0}$$

$$- 2L''(s_1^-)C_{+-}(\tilde{s}_1^{0+})E_{+0}(s_1, s_2, s_3)\Big]F_+^{(1)}(M_\pi, M_\pi, M_{\pi^0}, M_\pi, s_1)$$

$$- 8\Big[M_\eta L_1 D_{+-}\Big(C_{+0}(s_1) + E_{+0}^-(s_1, s_2, s_3)\Big)\frac{\mathbf{Q}_1^4}{(Q_1^0)^2} + \Big(L_1 C_{+-}(\tilde{s}_1^{0+})$$

$$- 2M_\eta L''(s_1^-)D_{+-}\Big)E_{+0}(s_1, s_2, s_3)\frac{\mathbf{Q}_1^2}{Q_1^0}\Big]F_+^{(2)}(M_\pi, M_\pi, M_{\pi^0}, M_\pi, s_1)$$

$$+ 16M_\eta L_1 D_{+-}E_{+0}(s_1, s_2, s_3)\frac{\mathbf{Q}_1^4}{(Q_1^0)^2}F_+^{(3)}(M_\pi, M_\pi, M_{\pi^0}, M_\pi, s_1)$$

$$+ 2K_0 C_x(\tilde{s}_1^{0+})\Big(C_{+0}(s_1) + E_{+0}^-(s_1, s_2, s_3)\Big)F_+(M_{\pi^0}, M_{\pi^0}, M_{\pi^0}, M_\pi, s_1)$$

$$- 4K_0\Big[M_\eta D_x\Big(C_{+0}(s_1) + E_{+0}^-(s_1, s_2, s_3)\Big)\frac{\mathbf{Q}_1^2}{Q_1^0} + C_x(\tilde{s}_1^{0+})E_{+0}(s_1, s_2, s_3)\Big]$$

$$\times F_+^{(1)}(M_{\pi^0}, M_{\pi^0}, M_{\pi^0}, M_\pi, s_1)$$

$$+ 8M_\eta K_0 D_x E_{+0}(s_1, s_2, s_3)\frac{\mathbf{Q}_1^2}{Q_1^0}F_+^{(2)}(M_{\pi^0}, M_{\pi^0}, M_{\pi^0}, M_\pi, s_1) + (s_1 \leftrightarrow s_2)\Big\}$$

$$+ 2K_0 C_{00}(\tilde{s}_3^{00})C_x(s_3)F_0(M_{\pi^0}, M_{\pi^0}, M_{\pi^0}, M_{\pi^0}, s_3)$$

$$- 4M_\eta K_0 D_{00}C_x(s_3)\frac{\mathbf{Q}_3^2}{Q_3^0}F_0^{(1)}(M_{\pi^0}, M_{\pi^0}, M_{\pi^0}, M_{\pi^0}, s_3)$$

$$+ 4L''(s_3)C_x(\tilde{s}_3^{00})C_x(s_3)F_0(M_\pi, M_\pi, M_{\pi^0}, M_{\pi^0}, s_3)$$

$$+ 4\Big[L_1 C_x(\tilde{s}_3^{00}) - 2M_\eta L''(s_3)D_x\Big]C_x(s_3)\frac{\mathbf{Q}_3^2}{Q_3^0}F_0^{(1)}(M_\pi, M_\pi, M_{\pi^0}, M_{\pi^0}, s_3)$$

$$- 8M_\eta L_1 D_x C_x(s_3)\frac{\mathbf{Q}_3^4}{(Q_3^0)^2}F_0^{(2)}(M_\pi, M_\pi, M_{\pi^0}, M_{\pi^0}, s_3)$$

$$+ 8\Big[L'''_{+0}(s_3)C_{+0}(\tilde{s}_3^{+-})$$

$$- \frac{\Delta_\pi}{4M_{\pi^0}}\Big(\frac{s_3 + 2\mathbf{Q}_3^2}{2Q_3^0} - p_3^0\Big)L_0 E_{+0}\Big]C_{+-}(s_3)F_0(M_\pi, M_{\pi^0}, M_\pi, M_\pi, s_3)$$

$$- 8\Big[\frac{1}{2}L_1 C_{+0}(\tilde{s}_3^{+-}) + 2M_\eta L'''_{+0}(s_3)D_{+0}$$

$$- \frac{\Delta_\pi}{4M_{\pi^0}}L_0 E_{+0}\Big]C_{+-}(s_3)\frac{\mathbf{Q}_3^2}{Q_3^0}F_0^{(1)}(M_\pi, M_{\pi^0}, M_\pi, M_\pi, s_3)$$

$$+ 8M_\eta L_1 D_{+0}C_{+-}(s_3)\frac{\mathbf{Q}_3^4}{(Q_3^0)^2}F_0^{(2)}(M_\pi, M_{\pi^0}, M_\pi, M_\pi, s_3) , \tag{B.5}$$

$$\mathcal{M}_c^B = \Big\{4L'(s_1)C_{+0}^2(s_1)J_{+0}^2(s_1) + (s_1 \leftrightarrow s_2)\Big\} + K(s_3)C_{00}(s_3)C_x(s_3)J_{00}^2(s_3)$$

$$+ 2\Big[L(s_3)C_x^2(s_3) + K(s_3)C_x(s_3)C_{+-}(s_3)\Big]J_{+-}(s_3)J_{00}(s_3) + 4L(s_3)C_{+-}^2(s_3)J_{+-}^2(s_3) . \tag{B.6}$$

We have used the following abbreviations:

$$J_{ab}(s_i) = \frac{iq_{ab}(s_i)}{8\pi\sqrt{s_i}} , \qquad q_{ab}^2(s_i) = \frac{\lambda(s_i, M_a^2, M_b^2)}{4s_i} ,$$

$$C_n(s_i) = C_n + D_n(s_i - s_n^{\mathrm{thr}}) + F_n(s_i - s_n^{\mathrm{thr}}) ,$$

$$\tilde{s}_i^{cd} = M_c^2 + M_i^2 - s_i + \frac{M_\eta}{Q_i^0}(s_i + 2\mathbf{Q}_i^2 - M_c^2 + M_d^2) ,$$

$$\tilde{E}_{+0}(s_1, s_2, s_3) = E_{+0}\frac{q_{+0}^2(s_1)}{3s_1 M_\eta}\Big(s_1(s_3 - s_2) + \Delta_\pi(M_\pi^2 - M_\eta^2)\Big) ,$$

$$E_{+0}^{(\pm)}(s_1, s_2, s_3) = E_{+0}\Big[\frac{(s_1(\pm\Delta_\pi))(s_3 - s_2 + \Delta_\pi)}{2M_\eta Q_1^0} - \Delta_\pi\Big] ,$$

$$E_{+-}(s_1, s_2, s_3) = E_{+-}\frac{s_3(s_1 - s_2)}{2M_\eta Q_3^0} ,$$

$$K(s_i) = K_0 + K_1\Big[(p_i^0 - M_{\pi^0})^2 + 2\Big(\frac{Q_i^0}{2} - M_{\pi^0}\Big)^2 + \frac{\mathbf{Q}_i^2}{6}\Big(1 - \frac{4M_{\pi^0}^2}{s_i}\Big)\Big] ,$$

$$L(s_i) = L_0 + L_1(p_i^0 - M_{\pi^0}) + L_2(p_i^0 - M_{\pi^0})^2 + L_3\frac{\mathbf{Q}_i^2}{3}\Big(1 - \frac{4M_\pi^2}{s_i}\Big)$$

$$\tilde{L}(s_i) = L_1 + 2L_2\Big[\frac{Q_i^0}{2}\Big(1 - \frac{\Delta_\pi}{s_i}\Big) - M_{\pi^0}\Big] + 2L_3\Big[p_i^0 - \frac{Q_i^0}{2}\Big(1 + \frac{\Delta_\pi}{s_i}\Big)\Big]$$

$$L'(s_i) = L_0 + L_1\Big(\frac{Q_i^0}{2}\Big(1 - \frac{\Delta_\pi}{s_i}\Big) - M_{\pi^0}\Big) + L_2\Big[\Big(\frac{Q_i^0}{2}\Big(1 - \frac{\Delta_\pi}{s_i}\Big) - M_{\pi^0}\Big)^2 + \frac{\mathbf{Q}_i^2}{3s_i}q_{+0}^2(s_i)\Big]$$

$$+ L_3\Big[\Big(\frac{Q_i^0}{2}\Big(1 + \frac{\Delta_\pi}{s_i}\Big) - p_i^0\Big)^2 + \frac{\mathbf{Q}_i^2}{3s_i}q_{+0}^2(s_i)\Big] ,$$

$$L''(s_i^{(\pm)}) = L_0 + L_1\Big(\frac{s_i(\pm\Delta_\pi)}{2Q_i^0} - M_{\pi^0}\Big) ,$$

$$L'''_{ab}(s_i^{(\pm)}) = L_0 + L_1\Big(\frac{1}{2}(M_\eta - M_a - M_b) - \frac{s_i(\pm\Delta_\pi)}{4Q_i^0}\Big) . \tag{B.7}$$

In the notation, it is understood that the shape parameter term F_n is omitted in the polynomials $C_n(\tilde{s}_i^{cd})$ inside the "genuine" two-loop graphs. There is a subtlety with regard to the neutral Dalitz plot couplings in the irreducible two-loop graphs: since we included these couplings only up to $\mathcal{O}(\epsilon^2)$, the $\Delta I = 1$ rule is only fulfilled up that same order. Eq. (3.2), however, is valid up to $\mathcal{O}(\epsilon^4)$, so that we have to replace $K_0 \to \bar{K}_0 = -(3L_0 + L_1 Q_n)$ in $\mathcal{M}_n^A$ and $\mathcal{M}_c^A$ above or simply $\bar{K}_0 = \tilde{\mathcal{N}}_n(1 - \frac{4}{9}\tilde{b}M_\eta^2 Q_n^2)$. The numerical effects of this replacement are small.

$F_i(\ldots; s)$, $F_i^{(k)}(\ldots; s)$, $k = 1, 2, 3$, stand for the integral representations $F(\ldots; s)$, $F^{(k)}(\ldots; s)$, evaluated at $\mathbf{Q}_i^2 = \lambda(M_\eta^2, M_i^2, s_i)/4M_\eta^2$, with $i = 1, 2, 3$. The analytic expression for these two-loop functions read

$$F(M_a, M_b, M_c, M_d, s) = \mathcal{N}\Big[2A\,f_1 + B\,f_0 - \frac{3\mathbf{Q}^2}{10s}(B\,f_1 + 2C\,f_0)$$
$$+ \mathcal{K}(X_3 f_3 + X_2 f_2 + X_1 f_1 + X_0 f_0)\Big]\,,$$

$$F^{(1)}(M_a, M_b, M_c, M_d, s) = \frac{\mathcal{N}}{10}(1+\delta)\big[(10A - B)f_1 + (5B - 2C)f_0\big] + \mathcal{O}(\epsilon^4)\,,$$

$$F^{(2)}(M_a, M_b, M_c, M_d, s) = \frac{\mathcal{N}}{2}\bigg[-\frac{1}{\mathbf{Q}^2}\Big(2A^2 f_3 + 3AB f_2 + (B^2 - 2AC)f_1 + BC f_0\Big)$$
$$+ \frac{(1+\delta)^2}{4}\Big(A f_3 + (B - 2A)f_2 + (4A - 2B + C)f_1 + 2(B - C)f_0\Big)\bigg] + \mathcal{O}(\epsilon^4)\,,$$

$$F^{(3)}(M_a, M_b, M_c, M_d, s) = \frac{\mathcal{N}(1+\delta)}{16}\bigg[\frac{3}{\mathbf{Q}^2}\Big(A^2 f_4 + 2A(B - 4A)f_3$$
$$+ (2AC + B^2 - 12AB)f_2 + (2BC - 8AC - 4B^2)f_1 + (C^2 - 4BC)f_0\Big)$$
$$- (1+\delta)^2\Big(A f_4 + (B - 3A)f_3 + (3A - 3B + C)f_2$$
$$+ (3B - 4A - 3C)f_1 + (3C - 2B)f_0\Big)\bigg] + \mathcal{O}(\epsilon^4)\,, \tag{B.8}$$

with

$$f_2 = -\frac{1}{5A}(3B f_1 + C f_0)\,, \qquad f_3 = -\frac{1}{7A^2}\Big[3(AC - B^2)f_1 - BC f_0\Big]\,,$$
$$f_4 = \frac{1}{9A^2}\Big[3(ABC + 5BC - 5B^3)f_1 - 5(B^2 C - C^2)f_0\Big]\,,$$
$$X_0 = HBC - RC\,, \quad X_1 = H(2AC + B^2) - R(2B - C)\,, \quad X_2 = 3HAB - R\Big(3A - \frac{3}{2}B\Big)\,,$$
$$X_3 = 2HA^2 + 2AR\,, \quad H = -\frac{3}{2}\Big(1 + \frac{\mathbf{Q}^2}{3s}\Big)\,, \quad R = \frac{\mathbf{Q}^2 Q_0^2}{2s}(1 + \tilde{\delta})^2\,. \tag{B.9}$$

and

$$\mathcal{N} = \frac{1}{256\pi^3 \sqrt{s}}\,\frac{\lambda^{1/2}(s_0, M_a^2, M_b^2)}{s_0\sqrt{\Delta^2 - \frac{(1+\tilde{\delta})^2}{4}\mathbf{Q}^2}}\,,$$

$$\mathcal{K} = \bigg[\frac{1}{2(M_\eta^2 + M_c^2) - (M_a + M_b)^2 - s_0} + \frac{1}{s_0 - (M_a - M_b)^2} - \frac{2}{s_0}\bigg]\frac{M_\eta^2}{s_0 - M_\eta^2 - M_c^2}\,,$$

$$f_0 = 4\big(v_1 + v_2 - \bar{v}_2 + h\big) \; ,$$

$$f_1 = \frac{4}{3}\big(y_1(v_1 - 1) + y_2(v_2 - 1) - \bar{y}_2(\bar{v}_2 - 1) + h\big) \; ,$$

$$h = \frac{1}{2}\ln\left(\frac{1 + \mathbf{Q}^2/s}{1 + \bar{\mathbf{Q}}^2/\bar{s}}\right) \; , \quad \bar{\mathbf{Q}}^2 = \mathbf{Q}^2(\bar{s}) \; , \quad \bar{s} = (M_c + M_d)^2 \; ,$$

$$v_i = \sqrt{-y_i}\arctan\frac{1}{\sqrt{-y_i}} \; , \quad i = 1, 2 \; ; \quad \bar{v}_2 = \sqrt{-\bar{y}_2}\arctan\frac{1}{\sqrt{-\bar{y}_2}} \; ,$$

$$y_{1,2} = \frac{-B \mp \sqrt{B^2 - 4AC}}{2A} \; , \quad \bar{y}_2 = y_2(\bar{s}) \; ,$$

$$A = -\frac{\mathbf{Q}^2}{s}(M_c^2 + \Delta^2) \; , \quad B = q_0^2 - \Delta^2 + \frac{\mathbf{Q}^2}{s}M_c^2 \; , \quad C = -q_0^2 \; ,$$

$$s_0 = M_\eta^2 + M_c^2 - 2M_\eta\left(M_c^2 + \frac{\mathbf{Q}^2(1 + \tilde{\delta})^2}{4}\right)^{1/2} \; , \quad q_0^2 = \frac{\lambda(s, M_c^2, M_d^2)}{4s} \; ,$$

$$\Delta^2 = \frac{\lambda(M_\eta^2, M_c^2, (M_a + M_b)^2)}{4M_\eta^2} \; , \quad \tilde{\delta} = \frac{M_c^2 - M_d^2}{s} \; . \tag{B.10}$$

B.2 Resummed amplitudes

In order to estimate the effects of higher-order corrections we iterate the bubble diagrams and the external vertex of the non-trivial two-loop graph. A diagrammatic expression of this iteration is shown in Fig. 3. Here we show the results including isospin violation. For the bubble chain a coupled-channel resummation can be performed analogously to Ref. [62]. We obtain

$$\mathcal{M}_n^{\mathrm{u}}(s_1, s_2, s_3) = \frac{2L(s_1)C_x(s_1)J_{+-}(s_1) + K(s_1)\Big[C_{00}(s_1)J_{00}(s_1) - 2\chi(s_1)J_{+-}(s_1)J_{00}(s_1)\Big]}{1 - 2C_{+-}(s_1)J_{+-}(s_1) - C_{00}(s_1)J_{00}(s_1) + 2\chi(s_1)J_{+-}(s_1)J_{00}(s_1)}$$

$$+ (s_1 \leftrightarrow s_2) + (s_1 \leftrightarrow s_3) \; ,$$

$$\mathcal{M}_c^{\mathrm{u}}(s_1, s_2, s_3) = \frac{2C_{+0}(s_1)J_{+0}(s_1)L'(s_1)}{1 - 2C_{+0}(s_1)J_{+0}(s_1)} - \frac{\tilde{E}'_{+0}(s_1, s_2, s_3)\tilde{L}(s_1)J_{+0}(s_1)}{1 - E_{+0}(s_1)J_{+0}(s_1)} + (s_1 \leftrightarrow s_2)$$

$$+ \frac{2L(s_3)\Big[C_{+-}(s_3)J_{+-}(s_3) - 2\chi(s_3)J_{+-}(s_3)J_{00}(s_3)\Big] + K(s_3)C_x(s_3)J_{00}(s_3)}{1 - 2C_{+-}(s_3)J_{+-}(s_3) - C_{00}(s_3)J_{00}(s_3) + 2\chi(s_3)J_{+-}(s_3)J_{00}(s_3)} \; ,$$

$$\tag{B.11}$$

where

$$\chi(s_i) = C_{+-}(s_i)C_{00}(s_i) - C_x(s_i)^2 \; ,$$

$$\tilde{E}'_{+0}(s_1, s_2, s_3) = \Big[E_{+0} + G_{+0}(s_i - s_{+0}^{\mathrm{thr}})\Big]\frac{q_{+0}^2(s_1)}{3s_1 M_\eta}\Big(s_1(s_3 - s_2) + \Delta_\pi(M_\pi^2 - M_\eta^2)\Big) \; ,$$

$$E_{+0}(s_i) = \frac{4q_{+0}^2(s_i)}{3}\Big[E_{+0} + G_{+0}(s_i - s_{+0}^{\mathrm{thr}})\Big] \; , \qquad G_{+0} = 3\pi b_1 \; , \tag{B.12}$$

and b_1 is the P-wave effective range. Additionally, we performed a resummation of the external vertex of the non-trivial two-loop diagram. This can be achieved by replacing the
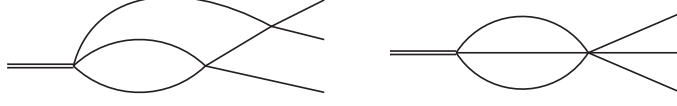
Figure 6: Two-loop graphs with three-particle cuts in the physical region.

outer vertex in Eqs. (B.4) and (B.6) according to

$$C_{00}(s_i) \to \frac{C_{00}(s_i) - 2\chi(s_i)J_{+-}(s_i)}{1 - C_{00}(s_i)J_{00}(s_i) - 2C_{+-}(s_i)J_{+-}(s_i) + 2\chi(s_i)J_{+-}(s_i)J_{00}(s_i)} \ ,$$

$$C_x(s_i) \to \frac{C_x(s_i)}{1 - C_{00}(s_i)J_{00}(s_i) - 2C_{+-}(s_i)J_{+-}(s_i) + 2\chi(s_i)J_{+-}(s_i)J_{00}(s_i)} \ ,$$

$$C_{+0}(s_i) \to \frac{C_{+0}(s_i)}{1 - 2C_{+0}(s_i)J_{+0}(s_i)} \ , \qquad E_{+0}^{(\pm)}(s_1, s_2, s_3) \to \frac{E'^{(\pm)}_{+0}(s_1, s_2, s_3)}{1 - E_{+0}(s_1)J_{+0}(s_1)} \ ,$$

$$C_{+-}(s_i) \to \frac{C_{+-}(s_i) - \chi(s_i)J_{00}(s_i)}{1 - C_{00}(s_i)J_{00}(s_i) - 2C_{+-}(s_i)J_{+-}(s_i) + 2\chi(s_i)J_{+-}(s_i)J_{00}(s_i)} \ , \qquad \text{(B.13)}$$

with

$$E'^{(\pm)}_{+0}(s_1, s_2, s_3) = \left[E_{+0} + G_{+0}(s_i - s_{+0}^{\text{thr}}) \right] \left[\frac{(s_1(\pm\Delta_\pi))(s_3 - s_2 + \Delta_\pi)}{2M_\eta Q_1^0} - \Delta_\pi \right] \ . \qquad \text{(B.14)}$$

C. Comment on imaginary parts of two-loop diagrams

In our analysis of the non-relativistic $\eta \to 3\pi$ decay amplitude, we have neglected the imaginary parts of the non-trivial two-loop graphs, see Fig. 6 (left). The loop function $F(s)$ (in the simplified notation introduced for the equal-mass case in Sect. 4) given in Appendix B.1 strictly speaking only corresponds to the *real* part of this diagram. At leading order in the ϵ expansion, its *imaginary* part is given by

$$\text{Im} \, F(s) = -\frac{1}{\sqrt{3}(32\pi)^2} \frac{(M_\eta - 3M_\pi)^2}{M_\pi^2} + \mathcal{O}(\epsilon^6) \ . \qquad \text{(C.1)}$$

We therefore confirm that $\text{Im} \, F(s) = \mathcal{O}(\epsilon^4)$, while the real part of the same diagram already starts at $\mathcal{O}(\epsilon^2)$. The imaginary part is due to the three-pion cut and only arises because the η is unstable, $M_\eta > 3M_\pi$. It stems from a part of the non-relativistic loop integral in which one of the propagators is non-singular, and therefore yields a result very similar to that of the sunset graph Fig. 6 (right), which in the non-relativistic framework can only arise when introducing (very small) six-pion vertices [29, 63]. The three-pion cut causes a non-vanishing imaginary part of the isospin amplitudes $\mathcal{M}_I(s)$ already at threshold $s = 4M_\pi^2$.

It is obvious that $\text{Im} \, F(s)$ can only contribute to the amplitude's squared modulus at $\mathcal{O}(a_{\pi\pi}^3\epsilon^5)$ via interference with one-loop terms, and is therefore naturally suppressed compared to the real part at two-loop order. What is less clear is its relative importance compared to the imaginary parts generated at three loops by the unitarization prescription Eq. (4.9). The latter contributes to $|\mathcal{M}|^2$ at $\mathcal{O}(a_{\pi\pi}^4\epsilon^4)$, i.e. it is suppressed in powers of $a_{\pi\pi}$, but enhanced in ϵ. By investigating the imaginary part of the dominant isospin $I = 0$

amplitude $\mathcal{M}_0(s)$, with Eq. (C.1) added appropriately to the representation Eq. (4.4), we find that the two-loop imaginary part is suppressed by more than a factor of 30 relative to the one-loop piece at the center of the Dalitz plot, and by roughly a factor of 2 relative to the three-loop part. This suppression grows even stronger when considering derivatives of the amplitude, as s-dependence in $\text{Im}\,F(s)$ is even further suppressed in ϵ, see Eq. (C.1). We therefore neglect these terms of $\mathcal{O}(ia_{\pi\pi}^2\epsilon^4)$ in our analysis, and consider their effects to be safely included in our error estimates due to partial higher-order resummation. The smallness of the imaginary parts due to three-pion cuts is in accordance with findings from ChPT at two loops [6] as well as from dispersion relations [22].

References

[1] D. G. Sutherland, *Current algebra and the decay $\eta \to 3\pi$*, Phys. Lett. **23** (1966) 384.

[2] J. S. Bell and D. G. Sutherland, *Current algebra and $\eta \to 3\pi$*, Nucl. Phys. B **4** (1968) 315.

[3] J. A. Cronin, *Phenomenological model of strong and weak interactions in chiral $U(3) \times U(3)$*, Phys. Rev. **161** (1967) 1483.

[4] H. Osborn and D. J. Wallace, *$\eta - \eta'$ mixing, $\eta \to 3\pi$ and chiral lagrangians*, Nucl. Phys. B **20** (1970) 23.

[5] J. Gasser and H. Leutwyler, *$\eta \to 3\pi$ to one loop*, Nucl. Phys. B **250** (1985) 539.

[6] J. Bijnens and K. Ghorbani, *$\eta \to 3\pi$ at two loops in chiral perturbation theory*, JHEP **0711** (2007) 030 [arXiv:0709.0230 [hep-ph]].

[7] R. Baur, J. Kambor and D. Wyler, *Electromagnetic corrections to the decays $\eta \to 3\pi$*, Nucl. Phys. B **460** (1996) 127 [arXiv:hep-ph/9510396].

[8] C. Ditsche, B. Kubis and U.-G. Meißner, *Electromagnetic corrections in $\eta \to 3\pi$ decays*, Eur. Phys. J. C **60** (2009) 83 [arXiv:0812.0344 [hep-ph]].

[9] W. B. Tippens *et al.* [Crystal Ball Collaboration], *Determination of the quadratic slope parameter in $\eta \to 3\pi^0$ decay*, Phys. Rev. Lett. **87** (2001) 192001.

[10] A. Abele *et al.* [Crystal Barrel Collaboration], *Decay dynamics of the process $\eta \to 3\pi^0$*, Phys. Lett. B **417** (1998) 193.

[11] D. Alde *et al.* [Serpukhov-Brussels-Annecy (LAPP) and Soviet-CERN Collaborations], *Neutral decays of the η meson*, Z. Phys. C **25** (1984) 225 [Yad. Fiz. **40** (1984) 1447].

[12] F. Ambrosino *et al.* [KLOE Collaboration], *Measurement of the $\eta \to 3\pi^0$ slope parameter α with the KLOE detector*, Phys. Lett. B **694** (2010) 16 [arXiv:1004.1319 [hep-ex]].

[13] M. Unverzagt *et al.* [Crystal Ball at MAMI, TAPS and A2 Collaborations], *Determination of the Dalitz plot parameter α for the decay $\eta \to 3\pi^0$ with the Crystal Ball at MAMI-B*, Eur. Phys. J. A **39** (2009) 169 [arXiv:0812.3324 [hep-ex]].

[14] S. Prakhov *et al.* [Crystal Ball at MAMI and A2 Collaborations], *Measurement of the slope parameter α for the $\eta \to 3\pi^0$ decay with the Crystal Ball at MAMI-C*, Phys. Rev. C **79** (2009) 035204 [arXiv:0812.1999 [hep-ex]].

[15] M. N. Achasov *et al.*, *Dynamics of $\eta \to 3\pi^0$ decay*, JETP Lett. **73** (2001) 451 [Pisma Zh. Eksp. Teor. Fiz. **73** (2001) 511].

[16] M. Bashkanov *et al.* [CELSIUS-WASA Collaboration], *Measurement of the slope parameter for the $\eta \to 3\pi^0$ decay in the $pp \to pp\eta$ reaction*, Phys. Rev. C **76** (2007) 048201 [arXiv:0708.2014 [nucl-ex]].

[17] C. Adolph *et al.* [WASA-at-COSY Collaboration], *Measurement of the $\eta \to 3\pi^0$ Dalitz plot distribution with the WASA detector at COSY*, Phys. Lett. B **677** (2009) 24 [arXiv:0811.2763 [nucl-ex]].

[18] A. Neveu and J. Scherk, *Final-state interaction and current algebra in $K \to 3\pi$ and $\eta \to 3\pi$ decays*, Annals Phys. **57** (1970) 39.

[19] C. Roiesnel and T. N. Truong, *Resolution of the $\eta \to 3\pi$ problem*, Nucl. Phys. B **187** (1981) 293.

[20] J. Kambor, C. Wiesendanger and D. Wyler, *Final state interactions and Khuri–Treiman equations in $\eta \to 3\pi$ decays*, Nucl. Phys. B **465** (1996) 215 [arXiv:hep-ph/9509374].

[21] A. V. Anisovich and H. Leutwyler, *Dispersive analysis of the decay $\eta \to 3\pi$*, Phys. Lett. B **375** (1996) 335 [arXiv:hep-ph/9601237].

[22] G. Colangelo, S. Lanz and E. Passemar, *A new dispersive analysis of $\eta \to 3\pi$*, PoS **CD09** (2009) 047 [arXiv:0910.0765 [hep-ph]].

[23] M. Zdráhal, K. Kampf, M. Knecht and J. Novotný, *Construction of the $\eta \to 3\pi$ (and $K \to 3\pi$) amplitudes using dispersive approach*, PoS **CD09** (2009) 122 [arXiv:0910.1721 [hep-ph]].

[24] J. Bijnens and J. Gasser, *η decays at and beyond p^4 in chiral perturbation theory*, Phys. Scripta **T99** (2002) 34 [arXiv:hep-ph/0202242].

[25] B. Borasoy and R. Nißler, *Hadronic η and η' decays*, Eur. Phys. J. A **26** (2005) 383 [arXiv:hep-ph/0510384].

[26] M. Kolesár, *$\eta \to 3\pi$ in resummed χPT*, talk given at: EuroFlavour2010, Munich, Germany, September 8–10, 2010.

[27] F. Ambrosino *et al.* [KLOE Collaboration], *Determination of $\eta \to \pi^+\pi^-\pi^0$ Dalitz plot slopes and asymmetries with the KLOE detector*, JHEP **0805** (2008) 006 [arXiv:0801.2642 [hep-ex]].

[28] M. Unverzagt [Crystal Ball at MAMI Collaboration], *η and η' Physics at MAMI*, Nucl. Phys. Proc. Suppl. **198** (2010) 174 [arXiv:0910.1331 [hep-ex]].

[29] G. Colangelo, J. Gasser, B. Kubis and A. Rusetsky, *Cusps in $K \to 3\pi$ decays*, Phys. Lett. B **638** (2006) 187 [arXiv:hep-ph/0604084].

[30] M. Bissegger, A. Fuhrer, J. Gasser, B. Kubis and A. Rusetsky, *Cusps in $K_L \to 3\pi$ decays*, Phys. Lett. B **659** (2008) 576 [arXiv:0710.4456 [hep-ph]].

[31] M. Bissegger, A. Fuhrer, J. Gasser, B. Kubis and A. Rusetsky, *Radiative corrections in $K \to 3\pi$ decays*, Nucl. Phys. B **806** (2009) 178 [arXiv:0807.0515 [hep-ph]].

[32] C.-O. Gullström, A. Kupść and A. Rusetsky, *Predictions for the cusp in $\eta \to 3\pi^0$ decay*, Phys. Rev. C **79** (2009) 028201 [arXiv:0812.2371 [hep-ph]].

[33] B. Kubis and S. P. Schneider, *The cusp effect in $\eta' \to \eta\pi\pi$ decays*, Eur. Phys. J. C **62** (2009) 511 [arXiv:0904.1320 [hep-ph]].

[34] A. Fuhrer, *Pion photoproduction in a nonrelativistic theory*, Phys. Lett. B **683** (2010) 172 [arXiv:0909.3121 [hep-ph]].

[35] A. Fuhrer, *Pion electroproduction in a nonrelativistic theory*, Phys. Lett. B **692** (2010) 130 [arXiv:1007.0031 [hep-ph]].

[36] B. Kubis, *Cusp effects in meson decays*, EPJ Web Conf. **3** (2010) 01008 [arXiv:0912.3440 [hep-ph]].

[37] U.-G. Meißner, G. Müller and S. Steininger, *Virtual photons in SU(2) chiral perturbation theory and electromagnetic corrections to $\pi\pi$ scattering*, Phys. Lett. B **406** (1997) 154 [Erratum-ibid. B **407** (1997) 454] [arXiv:hep-ph/9704377].

[38] B. Ananthanarayan, G. Colangelo, J. Gasser and H. Leutwyler, *Roy equation analysis of $\pi\pi$ scattering*, Phys. Rept. **353** (2001) 207 [arXiv:hep-ph/0005297].

[39] G. Colangelo, J. Gasser and H. Leutwyler, *$\pi\pi$ scattering*, Nucl. Phys. B **603** (2001) 125 [arXiv:hep-ph/0103088].

[40] R. Kamiński, J. R. Peláez and F. J. Ynduráin, *The pion–pion scattering amplitude. III: Improving the analysis with forward dispersion relations and Roy equations*, Phys. Rev. D **77** (2008) 054015 [arXiv:0710.1150 [hep-ph]].

[41] J. Bijnens, G. Ecker and J. Gasser, *Chiral perturbation theory*, arXiv:hep-ph/9411232.

[42] K. Nakamura [Particle Data Group], *Review of particle physics*, J. Phys. G **37** (2010) 075021.

[43] J. Stern, H. Sazdjian and N. H. Fuchs, *What $\pi\pi$ scattering tells us about chiral perturbation theory*, Phys. Rev. D **47** (1993) 3814 [arXiv:hep-ph/9301244].

[44] M. Knecht, B. Moussallam, J. Stern and N. H. Fuchs, *The low-energy $\pi\pi$ amplitude to one and two loops*, Nucl. Phys. B **457** (1995) 513 [arXiv:hep-ph/9507319].

[45] H. Leutwyler, *Physics of the light quarks*, arXiv:0808.2825 [hep-ph].

[46] J. R. Batley *et al.*, *Determination of the S-wave $\pi\pi$ scattering lengths from a study of $K^{\pm} \to \pi^{\pm}\pi^0\pi^0$ decays*, Eur. Phys. J. C **64** (2009) 589 [arXiv:0912.2165 [hep-ex]].

[47] M. Knecht and R. Urech, *Virtual photons in low energy $\pi\pi$ scattering*, Nucl. Phys. B **519** (1998) 329 [arXiv:hep-ph/9709348].

[48] M. Knecht and A. Nehme, *Electromagnetic corrections to charged pion scattering at low energies*, Phys. Lett. B **532** (2002) 55 [arXiv:hep-ph/0201033].

[49] A. Abele *et al.* [Crystal Barrel Collaboration], *Momentum dependence of the decay $\eta \to \pi^+\pi^-\pi^0$*, Phys. Lett. B **417** (1998) 197.

[50] J. G. Layter, J. A. Appel, A. Kotlewski, W. Y. Lee, S. Stein and J. J. Thaler, *Study of Dalitz plot distributions of the decays $\eta \to \pi^+\pi^-\pi^0$ and $\eta \to \pi^+\pi^-\gamma$*, Phys. Rev. D **7**, 2565 (1973).

[51] G. D'Ambrosio, G. Isidori, A. Pugliese and N. Paver, *Strong rescattering in $K \to 3\pi$ decays and low-energy meson dynamics*, Phys. Rev. D **50** (1994) 5767 [Erratum-ibid. D **51** (1995) 3975] [arXiv:hep-ph/9403235].

[52] M. Gormley, E. Hyman, W. Y. Lee, T. Nash, J. Peoples, C. Schultz and S. Stein, *Experimental determination of the Dalitz plot distribution of the decays $\eta \to \pi^+\pi^-\pi^0$ and $\eta \to \pi^+\pi^-\gamma$, and the branching ratio $\eta \to \pi^+\pi^-\gamma/\eta \to \pi^+\pi^-\pi^0$*, Phys. Rev. D **2** (1970) 501.

[53] G. Amelino-Camelia *et al.*, *Physics with the KLOE-2 experiment at the upgraded DAϕNE*, Eur. Phys. J. C **68** (2010) 619 [arXiv:1003.3868 [hep-ex]].

[54] P. Adlarson and M. Zieliński [for the WASA-at-COSY Collaboration], *Measurement of the* $\eta \to \pi^+\pi^-\pi0$ *decay with WASA-at-COSY detector*, arXiv:1009.5508 [hep-ex].

[55] J. Gasser and H. Leutwyler, *Chiral perturbation theory to one loop*, Annals Phys. **158** (1984) 142.

[56] S. Necco, *Chiral low-energy constants from lattice QCD*, PoS **CONFINEMENT8** (2008) 024 [arXiv:0901.4257 [hep-lat]].

[57] C. Haefeli, M. A. Ivanov and M. Schmid, *Electromagnetic low-energy constants in ChPT*, Eur. Phys. J. C **53** (2008) 549 [arXiv:0710.5432 [hep-ph]].

[58] B. Moussallam, *A sum rule approach to the violation of Dashen's theorem*, Nucl. Phys. B **504** (1997) 381 [arXiv:hep-ph/9701400].

[59] B. Ananthanarayan and B. Moussallam, *Four-point correlator constraints on electromagnetic chiral parameters and resonance effective Lagrangians*, JHEP **0406** (2004) 047 [arXiv:hep-ph/0405206].

[60] J. Gasser and H. Leutwyler, *Chiral perturbation theory: expansions in the mass of the strange quark*, Nucl. Phys. B **250** (1985) 465.

[61] R. Urech, *Virtual photons in chiral perturbation theory*, Nucl. Phys. B **433** (1995) 234 [arXiv:hep-ph/9405341].

[62] G. Colangelo, J. Gasser and A. Rusetsky, *Isospin breaking in* K_{l4} *decays*, Eur. Phys. J. C **59** (2009) 777 [arXiv:0811.0775 [hep-ph]].

[63] J. Gasser, B. Kubis and A. Rusetsky, in preparation.